SIAM J. NUMER. ANAL.
Vol. 41, No. 3, pp. 1163–1194

SURFACE PRESSURE POISSON EQUATION FORMULATION OF THE PRIMITIVE EQUATIONS: NUMERICAL SCHEMES*

ROGER SAMELSON†, ROGER TEMAM‡, CHENG WANG‡, AND SHOUHONG WANG‡

Abstract. Numerical methods for the primitive equations (PEs) of oceanic flow are presented in this paper. First, a two-dimensional Poisson equation with a suitable boundary condition is derived to solve the surface pressure. Consequently, we derive a new formulation of the PEs in which the surface pressure Poisson equation replaces the nonlocal incompressibility constraint, which is known to be inconvenient to implement. Based on this new formulation, backward Euler and Crank–Nicolson schemes are presented. The marker and cell scheme, which gives values of physical variables on staggered mesh grid points, are chosen as spatial discretization. The convergence analysis of the fully discretized scheme is established in detail. The accuracy check for the scheme is also shown.

Key words. the primitive equations, surface pressure, staggered grid, convergence analysis

AMS subject classifications. 35Q35, 65M06, 86A10

DOI. 10.1137/S0036142901396284

Introduction. The primary purpose of this paper is to propose and analyze numerical methods for the three-dimensional (3-D) primitive equations (PEs) of large scale oceanic flow using the surface pressure Poisson equation with a suitable boundary condition.

The hydrostatic balance results in the decomposition of the total pressure field into two parts: the integral of the density variable in the vertical direction, and the pressure field at surface level $z = 0$, i.e., the surface pressure. It was shown by Lions, Temam, and Wang [13] that the surface pressure is the Lagrange multiplier of an incompressibility constraint (namely, the vertically averaged horizontal velocity is divergence-free). Based on this remark, they introduced a new mathematical formulation of the PEs in which the surface pressure disappears by projecting the PEs onto the function space of the divergence-free averaged horizontal velocity field.

In this paper, the preoccupations are different: we want to develop numerical algorithms for the solution of the PEs. Contrary to the approach in [13], the surface pressure will play a central role in the algorithm; it is dynamically updated in the momentum equation, instead of being treated as a Lagrange multiplier. In particular, we will display a Poisson equation for the surface pressure and derive an approximate boundary condition for this Poisson equation. As a result, the surface pressure Poisson equation replaces the nonlocal constraint for the horizontal velocity field. The vertical velocity is calculated by integrating the horizontal divergence of the horizontal velocity field, due to the 3-D incompressibility.

Numerical methods are then proposed for the PEs formulated in the surface pres-

*Received by the editors October 10, 2001; accepted for publication (in revised form) January 6, 2003; published electronically July 30, 2003.
http://www.siam.org/journals/sinum/41-3/39628.html

†College of Oceanic and Atmospheric Sciences, Oregon State University, 104 Ocean Admin. Bldg, Corvallis, OR 97331-5503 (rsamelson@oce.orst.edu). The research of this author was supported in part by ONR grant N00014-98-1-0813 and by the NSF under grant OCE-9907854.

‡Department of Mathematics and Institute for Scientific Computing and Applied Mathematics, Indiana University, Rawles Hall, Bloomington, IN 47405-5701 (temam@indiana.edu, cwang@indiana.edu, showang@indiana.edu). The research of the second author was supported by NSF grant DMS-0074334 and the Research Fund of Indiana University. The research of the fourth author was supported in part by ONR grant N00014-96-1-0425 and by NSF grant DMS-0072612.

sure Poisson equation. At each time step, the surface pressure field is determined by a two-dimensional (2-D) Poisson solver after the data of the horizontal velocity field and the density field are updated by the momentum equations and the density equations. In turn, the gradient of the surface pressure is updated at the next time step. The temporal discretization is implemented by either the backward Euler or the Crank–Nicolson method. For the spatial discretization, we adopt the idea of the 3-D marker and cell (MAC) grid. Different variables in the PEs are evaluated on different staggered grids. The derivatives are replaced by second order centered-difference operators, while the integration in the vertical direction is implemented by the trapezoidal rule. Following the approach related to the development of a local vorticity boundary condition, we derive a consistent and second order accurate boundary condition for the surface pressure at the discrete level. The main advantage of the MAC scheme can be seen in the fact that the computed horizontal velocity field has exactly zero mean-divergence in a discrete level. Because of such a property, the 3-D calculated velocity field is orthogonal to the horizontal and vertical gradients of the total pressure field in a discrete L^2 space, which plays an important role in the convergence analysis. The idea is similar to that of the finite element approach, yet it dramatically simplifies the computation. To our knowledge, this is the first theoretical analysis of the PEs on the MAC grid (which is usually referred to as a "C grid" in the geophysical fluid dynamics (GFD) literature). It should be possible to use similar methods to analyze other related GFD models.

The paper is organized as follows. In section 1 we recall the formulation of the PEs and introduce the alternate formulation using the surface pressure Poisson equation. Backward Euler and Crank–Nicolson schemes (in temporal discretization) are presented in section 2. The description of the 3-D MAC scheme is given in section 3, and the detailed convergence analysis of the backward Euler method combined with the MAC staggered grid is provided in section 4. Finally, a numerical accuracy check is given in section 5, using a set of exact solutions to compare with the profiles computed by our scheme.

1. The PEs and the surface pressure Poisson equation. We start with the nondimensional PEs with proper scaling:

(1.1)
$$\begin{cases} \boldsymbol{v}_t + (\boldsymbol{v}\cdot\nabla)\boldsymbol{v} + w\dfrac{\partial \boldsymbol{v}}{\partial z} + \dfrac{f}{Ro}k\times\boldsymbol{v} + \dfrac{1}{Ro}\left(\displaystyle\int_z^0 \nabla\rho(x,y,s)\,ds + \nabla p_s\right) = L_1\boldsymbol{v}, \\ \rho_t + (\boldsymbol{v}\cdot\nabla)\rho + w\dfrac{\partial\rho}{\partial z} = L_2\rho, \\ \nabla\cdot\displaystyle\int_{-H_0}^0 \boldsymbol{v}\,dz = 0. \end{cases}$$

See, e.g., Pedlosky [19] and Lions, Temam, and Wang [12, 13] for a detailed derivation. In the above system, $\boldsymbol{u} = (\boldsymbol{v}, w) = (u, v, w)$ is the 3-D velocity vector field, $\boldsymbol{v} = (u, v)$ the horizontal velocity, $w = \mathcal{W}(\boldsymbol{v})$ the vertical velocity in which the operator $\mathcal{W}$ will be introduced in (1.7), ρ the density field, p_s the surface pressure, and Ro a Rossby number. The term $fk\times\boldsymbol{v}$ corresponds to the Coriolis force in its β-plane approximation, with the parameter $f = f_0 + \beta y$. The operators ∇, $\nabla\cdot$, $\triangle$ represent the gradient, divergence, and Laplacian in the (x, y)-plane, respectively. The diffusion operators are given by $L_1 = (\frac{1}{Re_1}\triangle + \frac{1}{Re_2}\partial_z^2)$ and $L_2 = (\frac{1}{Rt_1}\triangle + \frac{1}{Rt_2}\partial_z^2)$. For simplicity, we denote $\nu_1 = \frac{1}{Re_1}$, $\nu_2 = \frac{1}{Re_1}$, $\kappa_1 = \frac{1}{Rt_1}$, $\kappa_2 = \frac{1}{Rt_1}$. The computational domain is

taken as $\mathcal{M} = \mathcal{M}_0 \times [-H_0, 0]$, where $\mathcal{M}_0$ is the surface part of the ocean. The boundary condition for (1.1) is given by

$$\begin{aligned} &\nu_2 \frac{\partial \boldsymbol{v}}{\partial z} = \tau_0, \quad \kappa_2 \frac{\partial \rho}{\partial z} = \rho_f \quad \text{at } z = 0, \\ &\nu_2 \frac{\partial \boldsymbol{v}}{\partial z} = 0, \quad \kappa_2 \frac{\partial \rho}{\partial z} = 0 \quad \text{at } z = -H_0, \end{aligned} \tag{1.2}$$

$$\boldsymbol{v} = 0 \quad \text{and} \quad \frac{\partial \rho}{\partial \boldsymbol{n}} = 0 \quad \text{on } \partial\mathcal{M}_0 \times [-H_0, 0], \tag{1.3}$$

in which the term τ_0 represents the wind stress force and ρ_f represents the heat flux at the surface of the ocean.

Furthermore, the PEs (1.1) are supplemented with the following initial data:

$$\boldsymbol{v}(x, y, z, 0) = \boldsymbol{v}_0(x, y, z), \quad \rho(x, y, z, 0) = \rho_0(x, y, z), \tag{1.4}$$

in which $\boldsymbol{v}_0$ satisfies the mean divergence-free property as will be stated below.

The momentum equation for the horizontal velocity $\boldsymbol{v}$ comes from its original form

$$\boldsymbol{v}_t + (\boldsymbol{v}\cdot\nabla)\boldsymbol{v} + w\frac{\partial \boldsymbol{v}}{\partial z} + \frac{1}{Ro}\Big(fk \times \boldsymbol{v} + \nabla p\Big) = \Big(\nu_1 \triangle + \nu_2 \partial_z^2\Big)\boldsymbol{v}, \tag{1.5}$$

combined with the hydrostatic balance

$$\frac{\partial p}{\partial z} = -\rho, \qquad \text{which implies} \qquad p(x, y, z) = \int_z^0 \rho(x, y, s)\, ds + p_s(x, y). \tag{1.6}$$

We note that p denotes the total pressure field; the surface pressure $p_s(x, y) = p(x, y, 0)$ is a 2-D field in the horizontal plane. We refer the readers to [3, 20, 24] for other physical and numerical considerations related to surface pressure.

The representation formula for the vertical velocity w comes from the vertical integration of the continuity equation $\nabla\cdot\boldsymbol{v} + \partial_z w = 0$, using the vanishing boundary condition for w at the top ($z = 0$) and at the bottom ($z = -H_0$):

$$w(x, y, z) = -\nabla\cdot \int_{-H_0}^{z} \boldsymbol{v}(x, y, s)\, ds \equiv \mathcal{W}(\boldsymbol{v}). \tag{1.7}$$

It was first observed by Lions, Temam, and Wang in [13] that the surface pressure appears to be the Lagrange multiplier of the nonlocal constraint $\nabla\cdot\int_{-H_0}^{0} \boldsymbol{v}\, dz = 0$. For instance, in view of studying the balance of energy of the system, we multiply the first equation in (1.1) by $\boldsymbol{v}$; then the integral $\int_{\mathcal{M}} \boldsymbol{v}\cdot\nabla p_s\, d\boldsymbol{x}$ vanishes.

1.1. Determination of the surface pressure variable. A major difficulty in the numerical approximation of the PEs is the absence of a time evolution equation for the surface pressure field. The main objective in this section is to derive an alternate formulation equivalent to the usual formulation (1.1) such that the surface pressure variable p_s can be determined by the horizontal velocity field $\boldsymbol{v}$ and the density field ρ, which can be updated by the momentum equations and the density equations. Some earlier work on this issue can be found in [1, 2, 4, 5, 7, 8, 11, 14, 15, 16, 18, 21, 22, 23, 25, 26].

1.1.1. Surface pressure Poisson equation. We now derive an equation for the surface pressure function $p_s(x,y)$. The starting point is the nonlocal constraint $\nabla\cdot\int_{-H_0}^{0}\boldsymbol{v}\,dz=0$. By taking the horizontal divergence of the momentum equation in (1.1), integrating over $(-H_0,0)$ in the z-direction, dividing by H_0, and keeping in mind that p_s is a variable in the (x,y) plane, we arrive at the following equation:

$$\begin{aligned}(\partial_t-\nu_1\triangle)\Big(\overline{\nabla\cdot\boldsymbol{v}}\Big)-\nu_2\overline{\Big(\partial_z^2(\nabla\cdot\boldsymbol{v})\Big)}+\frac{1}{H_0}\int_{-H_0}^{0}\nabla\cdot\Big((\boldsymbol{v}\cdot\nabla)\boldsymbol{v}+w\frac{\partial\boldsymbol{v}}{\partial z}\Big)\,dz\\ +\frac{1}{Ro}\overline{\nabla\cdot\Big(fk\times\boldsymbol{v}\Big)}+\frac{1}{H_0}\,\frac{1}{Ro}\int_{-H_0}^{0}\int_{z}^{0}\triangle\rho(x,y,s)\,ds\,dz+\frac{1}{Ro}\triangle p_s=0,\end{aligned}\tag{1.8}$$

where $\overline{f}$ represents the average of the variable f in the z-direction. The first term in (1.8) vanishes, since $\overline{\nabla\cdot\boldsymbol{v}}$ is identically 0 in the horizontal domain. The second term turns out to be

$$\nu_2\,\overline{\Big(\partial_z^2(\nabla\cdot\boldsymbol{v})\Big)}=\frac{\nu_2}{H_0}\int_{-H_0}^{0}\partial_z^2(u_x+v_y)\,dz=\frac{\nu_2}{H_0}\Big(u_{zx}+v_{zy}\Big)\Big|_{-H_0}^{0}.\tag{1.9}$$

The boundary condition in (1.2) indicates that $(u_{zx}+v_{zy})=\frac{1}{\nu_2}(\partial_x(\tau_0)_1+\partial_y(\tau_0)_2)$ at $z=0$ and $(u_{zx}+v_{zy})=0$ at $z=-H_0$. Inserting (1.9) into (1.8) and setting $\tau_d=\nabla\cdot\tau_0)$ at $z=0$, which is a known function, we conclude that the surface pressure p_s solves the following Poisson equation:

$$\begin{aligned}\triangle p_s=\frac{Ro}{H_0}\,\nabla\cdot\tau_0-\frac{Ro}{H_0}\int_{-H_0}^{0}\nabla\cdot\Big((\boldsymbol{v}\cdot\nabla)\boldsymbol{v}+w\frac{\partial\boldsymbol{v}}{\partial z}+\frac{1}{Ro}(fk\times\boldsymbol{v})\Big)\,dz\\ -\frac{1}{H_0}\int_{-H_0}^{0}\int_{z}^{0}\triangle\rho(x,y,s)\,ds\,dz.\end{aligned}\tag{1.10}$$

The Poisson equation (1.10), together with the boundary condition described below, determines the surface pressure field by the velocity field and the density field without involving time derivative profiles.

1.1.2. Boundary condition for the surface pressure. Another point we have to emphasize is that there should be a boundary condition imposed for the surface pressure Poisson equation (1.10) if the Dirichlet boundary condition (1.3) for horizontal velocity field $\boldsymbol{v}$ is imposed on the lateral boundary section $\partial\mathcal{M}_0\times[-H_0,0]$.

Integrating the momentum equation in (1.1) over $(-H_0,0)$ in the z-direction and dividing by H_0 gives

$$\begin{aligned}\overline{\boldsymbol{v}}_t+\overline{\Big((\boldsymbol{v}\cdot\nabla)\boldsymbol{v}+w\frac{\partial\boldsymbol{v}}{\partial z}\Big)}+\frac{1}{Ro}\overline{fk\times\boldsymbol{v}}+\frac{1}{H_0}\,\frac{1}{Ro}\int_{-H_0}^{0}\int_{z}^{0}\nabla\rho(\cdot,s)\,ds\,dz\\ +\frac{1}{Ro}\nabla p_s=\nu_1\triangle\overline{\boldsymbol{v}}+\nu_2\overline{\partial_z^2\boldsymbol{v}},\end{aligned}\tag{1.11}$$

assuming that p_s is independent of the z-variable. On the lateral boundary $\partial\mathcal{M}_0\times[-H_0,0]$, the time marching term $\overline{\boldsymbol{v}}_t$ and all the convection terms vanish because of the no-penetration, no-slip boundary condition (the term $w\frac{\partial\boldsymbol{v}}{\partial z}$ disappears since $\frac{\partial\boldsymbol{v}}{\partial z}$ is zero on the boundary). The term $\overline{\partial_z^2\boldsymbol{v}}$ also vanishes, since $\partial_z^2\boldsymbol{v}$ is also 0 on $\partial\mathcal{M}_0\times[-H_0,0]$. Therefore, by taking the inner product of (1.11) with the unit normal vector field on

the boundary $\partial\mathcal{M}_0$ (of the 2-D domain $\mathcal{M}_0$), we arrive at the following boundary condition for the surface pressure:

$$\frac{\partial p_s}{\partial \boldsymbol{n}} = \nu_1 \, Ro \, \triangle \overline{\boldsymbol{v}} \cdot \boldsymbol{n} \quad \text{on} \quad \partial\mathcal{M}_0. \tag{1.12}$$

1.2. Alternate formulation of the PEs. We then have the following formulation, in which the nonlocal constraint $\nabla \cdot \int_{-H_0}^{0} \boldsymbol{v}\, dz = 0$ is replaced by the surface pressure Poisson equation and a mean divergence-free boundary condition for the horizontal velocity:

$$\boldsymbol{v}_t + (\boldsymbol{v}\cdot\nabla)\boldsymbol{v} + \mathcal{W}(\boldsymbol{v})\frac{\partial \boldsymbol{v}}{\partial z} + \frac{f}{Ro} k \times \boldsymbol{v} + \frac{1}{Ro}\left(\int_z^0 \nabla \rho(x,y,s)\, ds + \nabla p_s\right) = L_1 \boldsymbol{v}, \tag{1.13a}$$

$$\rho_t + (\boldsymbol{v}\cdot\nabla)\rho + \mathcal{W}(\boldsymbol{v})\frac{\partial \rho}{\partial z} = L_2 \rho, \tag{1.13b}$$

$$\begin{aligned} \triangle p_s = {} & \frac{Ro}{H_0}\,\tau_d - \frac{Ro}{H_0}\int_{-H_0}^{0} \nabla\cdot\Big((\boldsymbol{v}\cdot\nabla)\boldsymbol{v} + \mathcal{W}(\boldsymbol{v})\frac{\partial \boldsymbol{v}}{\partial z} + \frac{1}{Ro}(f k \times \boldsymbol{v})\Big)\, dz \\ & - \frac{1}{H_0}\int_{-H_0}^{0}\int_z^0 \triangle \rho(x,y,s)\, ds\, dz, \end{aligned} \tag{1.13c}$$

$$\begin{aligned} & \frac{\partial \boldsymbol{v}}{\partial z} = \frac{\tau_0}{\nu_2} \quad \text{at} \quad z = 0, \qquad \frac{\partial \boldsymbol{v}}{\partial z} = 0 \quad \text{at} \quad z = -H_0, \\ & \frac{\partial \rho}{\partial z} = \frac{\rho_f}{\kappa_2} \quad \text{at} \quad z = 0, \qquad \frac{\partial \rho}{\partial z} = 0 \quad \text{at} \quad z = -H_0, \\ & \boldsymbol{v} = 0 \quad \text{and} \quad \frac{\partial \rho}{\partial \boldsymbol{n}} = 0 \quad \text{on} \quad \partial\mathcal{M}_0 \times [-H_0, 0], \end{aligned} \tag{1.13d}$$

$$(\overline{\nabla\cdot\boldsymbol{v}}) = 0 \quad \text{on} \ \partial\mathcal{M}_0. \tag{1.13e}$$

PROPOSITION 1.1. *For* $\boldsymbol{v}, \rho \in L^\infty([0,T], H^3)$, $\partial_t \boldsymbol{v}, \partial_t \rho \in L^\infty([0,T], H^1)$, *the original formulation* (1.1)–(1.3) *of the PEs is equivalent to the alternate formulation* (1.13a)–(1.13e).

Proof. Assume $(\boldsymbol{v}, \rho, p_s)$ is a solution of (1.1)–(1.3). We observe that p_s satisfies the Poisson equation (1.13b), which can be obtained by taking the horizontal divergence of the momentum equation in (1.1) and averaging in the vertical direction as shown in the above derivation. In addition, taking the vertical derivative of the representation formula for the vertical velocity in (1.1) indicates that the horizontal velocity $\boldsymbol{v}$ satisfies the constraint $\overline{\nabla\cdot\boldsymbol{v}} = 0$. The usage of the regularity for $\boldsymbol{v} \in L^\infty([0,T], H^3)$ shows that $\boldsymbol{v}$ satisfies the additional boundary condition (1.13e). This concludes that $(\boldsymbol{v}, \rho, p_s)$ is also a solution of (1.13).

Conversely, assume $(\boldsymbol{v}, \rho, p_s)$ is a solution of (1.13). We need to show that $\overline{\nabla\cdot\boldsymbol{v}} = 0$. Taking the divergence of (1.13a) and integrating in the vertical direction leads to

$$\partial_t(\overline{\nabla\cdot\boldsymbol{v}}) - \nu_1 \triangle(\overline{\nabla\cdot\boldsymbol{v}}) = 0, \tag{1.14a}$$

since *all the other terms are canceled by the surface pressure Poisson equation.* Hence the heat equation (1.14a) for the scalar quantity $\overline{\nabla\cdot\boldsymbol{v}}$, together with the homogeneous initial data

$$(\overline{\nabla\cdot\boldsymbol{v}})(x,y,t=0)=0, \tag{1.14b}$$

and the additional mean divergence-free boundary condition for the horizontal velocity imposed by (1.13e),

$$(\overline{\nabla\cdot\boldsymbol{v}})=0 \quad \text{on } \partial\mathcal{M}_0, \tag{1.14c}$$

show that $(\overline{\nabla\cdot\boldsymbol{v}})=0$; namely, the third equation in (1.1) is satisfied for all $t>0$. Therefore, $(\boldsymbol{v},\rho,p_s)$ is also a solution of (1.1)–(1.3). That completes the proof of Proposition 1.1. □

Remark 1.2. The above arguments show that the system (1.13a)–(1.13e) implies the original system of PEs (1.1)–(1.3), and therefore it implies (1.12), a Neumann-type boundary condition for the surface pressure p_s, since (1.12) is derived from the momentum equation in (1.1). In other words, the boundary condition (1.12) must be satisfied by any solution of the system (1.13a)–(1.13e). For the computations, the additional boundary condition (1.13e), a mean divergence-free boundary condition for the horizontal velocity, is not convenient to use. Instead, we will replace it by (1.12), a boundary condition for the surface pressure, to solve for the Poisson equation (1.13b); note that we are not claiming that the systems are equivalent if we replace (1.13e) by (1.12), leaving (1.13a)–(1.13d) unchanged. However, as we show below, such an equivalence occurs in the case of the MAC scheme, the spatially discrete scheme that will be studied in section 3.

1.3. Analogy with the 2-D Navier–Stokes equations. It could be observed that the boundary condition (1.13e) is coupled with the surface pressure Poisson equation (1.13b) and the momentum equation (1.13a), (1.13d). In more detail, in the derived formulation (1.13), four boundary conditions are prescribed for the horizontal velocity field: $\frac{\partial\boldsymbol{v}}{\partial z}=\frac{\tau_0}{\nu_2}$ on $z=0$, $\frac{\partial\boldsymbol{v}}{\partial z}=0$ on $z=-H_0$, $\boldsymbol{v}=0$ on $\partial\mathcal{M}_0\times[-H_0,0]$, and $(\overline{\nabla\cdot\boldsymbol{v}})=0$ on $\partial\mathcal{M}_0$, while there is no boundary condition for the surface pressure p_s. This subtle fact appears in a similar way for the formulations of incompressible fluid equations, such as the Navier–Stokes equation (NSE). For example, the vorticity-stream function formulation of the 2-D NSE in a simply connected domain, which is also a derived formulation, can be written as

$$\begin{cases} \partial_t\omega+(\boldsymbol{v}\cdot\nabla)\omega=\nu\triangle\omega, \\ \triangle\psi=\omega, \\ u=-\partial_y\psi, \qquad v=\partial_x\psi, \end{cases} \tag{1.15}$$

where $\boldsymbol{v}=(u,v)$ denotes the 2-D velocity field, $\omega=\nabla\times\boldsymbol{u}=-\partial_y u+\partial_x v$ denotes the vorticity, and the no-penetration, no-slip boundary condition can be written in terms of the stream function ψ:

$$\psi=0, \quad \frac{\partial\psi}{\partial\mathbf{n}}=0 \qquad \text{on} \qquad \partial\mathcal{M}_0. \tag{1.16}$$

Similar to our derived formulation (1.13), in the coupled system (1.15) and (1.16), there are two boundary conditions for the stream function ψ (both Dirichlet and Neumann) and no explicit boundary condition for the vorticity ω. On the other

hand, updating the dynamic equation in (1.15) requires the vorticity boundary values; see [6, 10, 17, 18, 27, 28] for detailed description, derivation, and analysis of vorticity boundary conditions. A similar difficulty arises in the formulation (1.13): what boundary condition should be imposed to solve surface pressure p_s? Of course, the Neumann boundary condition (1.12) is a good choice to replace (1.13e); their equivalence is not claimed at the PDE level, as noted in Remark 1.2. However, in the MAC spatial discretization with a staggered grid described in section 3, the boundary condition $(\overline{\nabla \cdot \boldsymbol{v}})\ |_{\partial \mathcal{M}_0} = 0$ is converted by a second order accurate realization into the surface pressure boundary condition. Furthermore, in such a staggered grid, the equivalence between the derived boundary condition and the nonlocal constraint on the boundary as in (1.13e) can be fully proven.

Remark 1.3. The precise approximation of the pressure field via the pressure Poisson equation is a well-known difficulty in the incompressible flow calculation if the physical boundary condition is presented. The approach for solving the 2-D and 3-D NSEs by utilizing a local pressure boundary condition was recently introduced by Johnston and Liu in [11]. Some ideas in their paper can be adapted in our work.

Remark 1.4. The PEs with general boundary conditions or noncylindric domains were investigated in earlier literatures by Lions, Temam, and Wang [12, 13, 14, 15, 16] in a PDE level. The corresponding numerical methods can be accordingly derived using finite element approaches. We hope to report that issue in a future paper.

2. Temporal discretization. Two computational methods for the PEs in surface pressure Poisson equation formulation (1.13) are proposed in this section. The horizontal velocity field and the density field are updated by the momentum equation (1.13a) and the density equation (1.13b). The surface pressure field, which is essentially a Lagrange multiplier in a horizontal plane, is determined by a 2-D Poisson solver, using the information of the velocity field and the density field at the same time step (stage). Henceforth, the surface pressure gradient is treated as a force term in the dynamic evolution of the momentum equation in the next time step (the stage). As a result, the surface pressure term is decoupled from the diffusion term; thus the Stokes solver is avoided. That dramatically simplifies the computation.

For simplicity, we use implicit treatment of the diffusion terms in the momentum equation and the density equation, which makes the stability and convergence analysis of the numerical scheme easier to handle. The backward Euler scheme is chosen as the example of the first order method (in temporal discretization) and the Crank–Nicolson scheme as the second order version.

2.1. Backward Euler method. Given the velocity field $\boldsymbol{u}^n$, surface pressure field p_s^n, and density field ρ^n at time t^n, we update all the profiles at the time step t^{n+1} through the following procedure.

Step 1. The semi-implicit scheme for the momentum equation and the density equation is given, leaving the convection term and the surface pressure gradient explicit:

$$\text{(2.1a)}\quad \begin{cases} \dfrac{\boldsymbol{v}^{n+1}-\boldsymbol{v}^n}{\triangle t} + (\boldsymbol{v}^n\cdot\nabla)\boldsymbol{v}^n + \mathcal{W}(\boldsymbol{v}^n)\dfrac{\partial \boldsymbol{v}^n}{\partial z} + \dfrac{f}{Ro}k\times\boldsymbol{v}^n \\ \qquad\qquad + \dfrac{1}{Ro}\displaystyle\int_z^0 \nabla\rho^n(x,y,s)\,d + \dfrac{1}{Ro}\nabla p_s^n(x,y) = \Big(\nu_1\triangle + \nu_2\partial_z^2\Big)\boldsymbol{v}^{n+1}, \\ \dfrac{\rho^{n+1}-\rho^n}{\triangle t} + (\boldsymbol{v}^n\cdot\nabla)\rho^n + w^n\dfrac{\partial\rho^n}{\partial z} = \Big(\kappa_1\triangle + \kappa_2\partial_z^2\Big)\rho^{n+1}, \end{cases}$$

which are three standard Poisson-like equations, with the boundary condition

$$\begin{aligned}
&\frac{\partial \boldsymbol{v}^{n+1}}{\partial z} = \frac{\tau_0}{\nu_2}, \quad \frac{\partial \rho^{n+1}}{\partial z} = \frac{\rho_f}{\kappa_2} \quad \text{at } z = 0,\\
&\frac{\partial \boldsymbol{v}^{n+1}}{\partial z} = 0, \quad \frac{\partial \rho^{n+1}}{\partial z} = 0 \quad \text{at } z = -H_0,\\
&\boldsymbol{v}^{n+1} = 0 \quad \text{and} \quad \frac{\partial \rho^{n+1}}{\partial \boldsymbol{n}} = 0 \quad \text{on} \quad \partial\mathcal{M}_0 \times [-H_0, 0].
\end{aligned} \tag{2.1b}$$

Step 2. With all the velocity field $\boldsymbol{v}^{n+1}$, w^{n+1} at hand, we can solve for the surface pressure field at the time step t^{n+1} by the 2-D Poisson equation

(2.2a)

$$\begin{aligned}
\triangle p_s^{n+1} = {} & \frac{Ro}{H_0}\,\tau_d^{n+1} - \frac{1}{H_0}\int_{-H_0}^{0}\int_z^0 \triangle\rho^{n+1}(x,y,s)\,ds\,dz\\
& - \frac{Ro}{H_0}\int_{-H_0}^{0} \nabla\cdot\Big((\boldsymbol{v}^{n+1}\cdot\nabla)\boldsymbol{v}^{n+1} + \mathcal{W}(\boldsymbol{v}^{n+1})\frac{\partial \boldsymbol{v}^{n+1}}{\partial z} + \frac{1}{Ro}(fk\times\boldsymbol{v}^{n+1})\Big)\,dz,
\end{aligned}$$

supplemented with the derived boundary condition (1.12), as argued in Remark 1.2 and section 1.3:

$$\frac{\partial p_s^{n+1}}{\partial \boldsymbol{n}} = \nu_1\, Ro\, \triangle\overline{\boldsymbol{v}}^{n+1}\cdot\boldsymbol{n} \quad \text{on} \quad \partial\mathcal{M}_0. \tag{2.2b}$$

2.2. Crank–Nicolson method. The updating from time step t^n to t^{n+1} is carried out by the following steps.

Step 1. Solve for the momentum equations and the density equations

$$\begin{cases}
\dfrac{\boldsymbol{v}^{n+1}-\boldsymbol{v}^n}{\triangle t} + RHS1^{n+\frac12} + \dfrac{1}{Ro}\nabla p_s^{n+\frac12} = \dfrac12\Big(\nu_1\triangle + \nu_2\partial_z^2\Big)(\boldsymbol{v}^n + \boldsymbol{v}^{n+1}),\\
\dfrac{\rho^{n+1}-\rho^n}{\triangle t} + RHS2^{n+\frac12} = \dfrac12\Big(\kappa_1\triangle + \kappa_2\partial_z^2\Big)(\rho^n + \rho^{n+1}),
\end{cases} \tag{2.3}$$

using the boundary condition (2.1b), where

$$\begin{aligned}
RHS1^{n+\frac12} = {} & (\boldsymbol{v}^{n+\frac12}\cdot\nabla)\boldsymbol{v}^{n+\frac12} + \mathcal{W}(\boldsymbol{v}^{n+\frac12})\frac{\partial \boldsymbol{v}^{n+\frac12}}{\partial z} + \frac{f}{Ro}k\times\boldsymbol{v}^{n+\frac12}\\
& + \frac{1}{Ro}\int_z^0 \nabla\rho^{n+\frac12}(x,y,s)\,ds,\\
RHS2^{n+\frac12} = {} & (\boldsymbol{v}^{n+\frac12}\cdot\nabla)\rho^{n+\frac12} + \mathcal{W}(\boldsymbol{v}^{n+\frac12})\frac{\partial \rho^{n+\frac12}}{\partial z}.
\end{aligned} \tag{2.4}$$

The velocity and the density profiles $(\boldsymbol{u},\rho) = (\boldsymbol{v}, w, \rho)$, along with the surface pressure p_s, at the time step $t^{n+\frac12}$ are evaluated by second order explicit extrapolation in time

$$\boldsymbol{u}^{n+\frac12} = \frac32\boldsymbol{u}^n - \frac12\boldsymbol{u}^{n-1}, \quad \rho^{n+\frac12} = \frac32\rho^n - \frac12\rho^{n-1}, \quad p_s^{n+\frac12} = \frac32 p_s^n - \frac12 p_s^{n-1}. \tag{2.5}$$

Note that the system (2.3) is also composed of three standard Poisson-like equations.

Step 2. The surface pressure field at the time step t^{n+1} is solved by the 2-D Poisson equation (2.2a) with the derived boundary condition (2.2b), as in the second step of the backward Euler scheme.

3. Spatial discretization: MAC scheme. We consider hereafter the oceanic basin given by $\mathcal{M}_0 = [0,1]^2$ and assume for simplicity that $\triangle x = \triangle y = \triangle z = h$. The analysis of the spatial discretization with regular grids is quite difficult. In this paper, we consider the MAC staggered grid as spatial discretization. Some well-known difficulties in the numerical simulation of NSE, such as enforcement of the incompressibility condition and lack of proper evolutionary equation for the pressure and associate boundary condition, were elegantly resolved in the celebrated MAC scheme, which was first proposed by Harlow and Welch in [9]. For the system of the PEs, the 3-D MAC staggered grid is used in the computational method.

An illustration of the MAC mesh on the section $z_k = (k+1/2)\triangle z$ is given in Figure 3.1. The surface pressure variable p_s is evaluated at the square points $(i \pm 1/2, j \pm 1/2)$, the velocity u is evaluated at the triangle points $(i, j \pm 1/2, k \pm 1/2)$, the velocity v is evaluated at the circle points $(i \pm 1/2, j, k \pm 1/2)$, and the velocity w and the density function ρ are evaluated at the dot points $(i \pm 1/2, j \pm 1/2, k)$. The advantage of such a staggered grid is the convenience to assure the divergence-free property of the numerical velocity field, which can be observed later.

The following centered differences using different stencils at different grid points is introduced to facilitate the description below:

$$
\begin{aligned}
&D_x g(x) = \frac{g(x+\frac{1}{2}h) - g(x-\frac{1}{2}h)}{h}, \quad \tilde{D}_x g(x) = \frac{g(x+h) - g(x-h)}{2h}, \\
&D_x^2 g(x) = \frac{g(x-h) - 2g(x) + g(x+h)}{h^2},
\end{aligned}
\tag{3.1}
$$

which are second order approximations to ∂_x, ∂_x^2, respectively. The corresponding operators in y- and z-directions, such as D_y, $\tilde{D}_y$, D_y^2, D_z, $\tilde{D}_z$, D_z^2, can be defined in the same fashion.

The discrete divergence of the total velocity field $\boldsymbol{u}$ is evaluated at the square points:

$$
(\nabla_h \cdot \boldsymbol{u})_{i+1/2,j+1/2,k+1/2} = \Big(D_x u + D_y v + D_z w\Big)_{i+1/2,j+1/2,k+1/2}. \tag{3.2}
$$

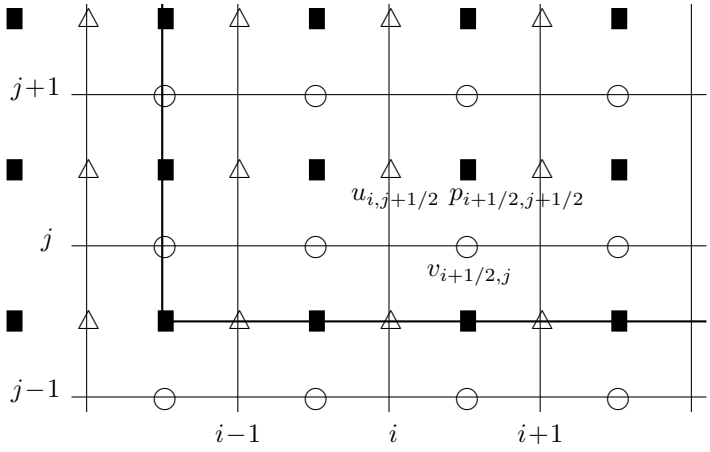

FIG. 3.1. *MAC mesh at* $z_k = (k+1/2)\triangle z$*; Harlow and Welch* [9].

The diffusion term for the velocity u is approximated by

$$\left(\nu_1\triangle+\nu_2\partial_z^2\right)u=\left(\nu_1\triangle_h+\nu_2D_z^2\right)u=\left(\nu_1(D_x^2+D_y^2)+\nu_2D_z^2\right)u \tag{3.3}$$

at $(i, j+1/2, k+1/2)$. The other diffusion terms, $\triangle_h v$, $D_z^2 v$, at the mesh point $(i+1/2, j, k+1/2)$, and $\triangle_h\rho$, $D_z^2\rho$, at the mesh point $(i+1/2, j+1/2, k)$, can be given in the same way. The gradient of density and the surface pressure appearing in the momentum equation is discretized by $(D_x\rho)_{i,j+1/2,k+1/2}$, $(D_y\rho)_{i,j+1/2,k+1/2}$ (and $(D_xp_s)_{i,j+1/2}$, $(D_yp_s)_{i+1/2,j}$), respectively.

The approximation to the nonlinear convection term $(\boldsymbol{v}\cdot\nabla)\boldsymbol{v}+w\frac{\partial\boldsymbol{v}}{\partial z}$, $(\boldsymbol{v}\cdot\nabla)\rho+w\frac{\partial\rho}{\partial z}$ at the corresponding mesh points for u, v, ρ relies on the introduction of average value of u, v, w at the staggered grid. For example, at the mesh point $(i, j+1/2, k+1/2)$ where u is located, the average v, w can be introduced as

$$\begin{aligned}\overline{v}_{i,j+1/2,k+1/2}=\ &\frac{1}{4}(v_{i-1/2,j,k+1/2}+v_{i+1/2,j,k+1/2}\\ &+v_{i-1/2,j+1,k+1/2}+v_{i+1/2,j+1,k+1/2}),\end{aligned} \tag{3.4a}$$

$$\begin{aligned}\overline{\overline{w}}_{i,j+1/2,k+1/2}=\ &\frac{1}{4}(w_{i-1/2,j+1/2,k}+w_{i+1/2,j+1/2,k}\\ &+w_{i-1/2,j+1/2,k+1}+w_{i+1/2,j+1/2,k+1}),\end{aligned} \tag{3.4b}$$

and the corresponding convection term for u: $uu_x+vu_y+wu_z$ can be defined as

$$\mathcal{N}_h(\boldsymbol{u},u)=u\tilde{D}_xu+\overline{\overline{v}}\tilde{D}_yu+\overline{\overline{w}}\tilde{D}_zu\qquad\text{at}\qquad(i,j+1/2,k+1/2). \tag{3.5}$$

The two other convection terms, $\mathcal{N}_h(\boldsymbol{u},v)_{i+1/2,j,k+1/2}$, $\mathcal{N}_h(\boldsymbol{u},\rho)_{i+1/2,j+1/2,k}$, which are approximations to $uv_x+vv_y+wv_z$, $u\rho_x+v\rho_y+w\rho_z$ at the corresponding mesh points, can be similarly defined. In addition, the Coriolis force term $fk\times\boldsymbol{v}=(-fv,fu)$ is evaluated at the mesh points for u, v, respectively, by taking the average of v and u at the required grid points as in (5.4):

$$\begin{aligned}(-fv)_{i,j+1/2,k+1/2}&=-f_{i,j+1/2}\overline{\overline{v}}_{i,j+1/2,k+1/2},\\ (fu)_{i+1/2,j,k+1/2}&=f_{i+1/2,j}\overline{\overline{u}}_{i+1/2,j,k+1/2}.\end{aligned} \tag{3.6}$$

Clearly, the truncation errors of these approximations are of second order. The momentum equation for u is implemented at triangle points, the second momentum equation is implemented at circle points, and the density equation is implemented at the mesh points $(i+1/2, j+1/2, k)$. The discrete version of the term $\int_z^0\nabla\rho(x,y,s)\,ds$ appearing in the momentum equation is a discrete integral of $\tilde{D}_x\rho$, $\tilde{D}_y\rho$ (which are defined at mesh points $(i, j+1/2, k)$, $(i+1/2, j, k)$, respectively, as given in (3.3)), in the z-direction. More accurately, $\mathcal{P}NRX$ is defined as the discrete version of $\int_z^0\rho_x(x,y,s)\,ds$:

$$\begin{aligned}\mathcal{P}NRX_{i,j+1/2,N-1/2}&=\frac{1}{2}\triangle z\,(D_x\rho)_{i,j+1/2,N},\\ \mathcal{P}NRX_{i,j+1/2,k-1/2}&=\mathcal{P}NRX_{i,j+1/2,k+1/2}+\triangle z\,(D_x\rho)_{i,j+1/2,k},\quad k\le N_z-1,\end{aligned} \tag{3.7a}$$

and $\mathcal{P}NRY$ can be given in a similar way:

(3.7b)
$$\mathcal{P}NRY_{i+1/2,j,N-1/2} = \frac{1}{2}\triangle z\,(D_y\rho)_{i+1/2,j,N},$$
$$\mathcal{P}NRY_{i+1/2,j,k-1/2} = \mathcal{P}NRY_{i+1/2,j,k+1/2} + \triangle z\,(D_y\rho)_{i+1/2,j,k}, \quad k \le N_z - 1.$$

Both formulae are second order approximation to the integral of the density gradient from z_k to 0.

The 2-D discrete Poisson equation for surface pressure p_s is implemented at square points. In more detail, we denote

$$\begin{aligned} \mathcal{F}U &= -\mathcal{N}_h(\boldsymbol{u},u) + \frac{1}{Ro}(fv) - \frac{1}{Ro}\mathcal{P}NRX \quad \text{at } (i,j+1/2,k+1/2), \\ \mathcal{F}V &= -\mathcal{N}_h(\boldsymbol{u},v) - \frac{1}{Ro}(fu) - \frac{1}{Ro}\mathcal{P}NRY \quad \text{at } (i+1/2,j,k+1/2) \end{aligned} \tag{3.8}$$

as the convection terms (including the Coriolis force term) for the momentum equation; therefore, the Poisson equation for surface pressure p_s can be written as

(3.9)
$$(\triangle_h p_s)_{i+1/2,j+1/2} = \frac{Ro}{H_0}\Big(D_x\tau_{0,1} + D_y\tau_{0,2}\Big)_{i+1/2,j+1/2} + Ro\,\overline{\mathcal{F}P}_{i+1/2,j+1/2}, \text{ where}$$
$$\mathcal{F}P_{i+1/2,j+1/2,k+1/2} = (D_x\mathcal{F}U)_{i+1/2,j+1/2,k+1/2} + (D_y\mathcal{F}V)_{i+1/2,j+1/2,k+1/2},$$

on the mesh points $(i+1/2, j+1/2)$ in the 2-D region $\mathcal{M}_0 = [0,1]^2$. The average of $\mathcal{F}P$, which is evaluated at the same numerical mesh grid as p, is defined as

$$\overline{\mathcal{F}P}_{i+1/2,j+1/2} = \frac{1}{H_0}\sum_{k=0}^{nz-1}(\triangle z\,\mathcal{F}P_{i+1/2,j+1/2,k+1/2}), \tag{3.10}$$

which is a second order approximation to the integral of $\mathcal{F}P$ in the z-direction. Such an evaluation of the discrete integral in the z-direction can be applied to any variable whose z-direction grid is indexed as $k \pm 1/2$.

It should be remarked that some suitable boundary condition is needed to solve the 2-D Poisson equation (3.9). Such a choice of the boundary condition assures the discrete divergence $(\nabla_h \cdot \boldsymbol{v})$ has mean zero (in the z-direction) on the boundary $\partial\mathcal{M}_0$. Details will be discussed in a later section.

On the physical boundary section $i = 0$, the no-penetration, no-slip boundary condition $\boldsymbol{v} = 0$ is translated by the reflection rule, whose application in the case of the 2-D NSE can be found in earlier work [4, 6, 7, 9],

$$u_{0,j+1/2,k+1/2} = 0, \quad v_{-1/2,j,k+1/2} + v_{1/2,j,k+1/2} = 0, \tag{3.11}$$

and the no-flux boundary condition for the density function is imposed by

$$(D_x\rho)_{0,j+1/2,k} = 0, \quad \text{which implies } \rho_{-1/2,j+1/2,k} = \rho_{1/2,j+1/2,k}. \tag{3.12}$$

Similarly, on the boundary section $j = 0$, the boundary condition $\boldsymbol{v} = 0$ is imposed by $v_{i+1/2,0,k+1/2} = 0$, $u_{i,-1/2,k+1/2} + u_{i,1/2,k+1/2} = 0$, and the boundary condition $\frac{\partial\rho}{\partial\boldsymbol{n}} = 0$ is imposed by $\rho_{i+1/2,-1/2,k} = \rho_{i+1/2,1/2,k}$.

On the bottom boundary $z = -H_0$, i.e., $k = 0$, the boundary condition $\frac{\partial \boldsymbol{v}}{\partial z} = 0$, $\frac{\partial \rho}{\partial z} = 0$ can be written as

$$\begin{aligned} &u_{i,j+1/2,-1/2} = u_{i,j+1/2,1/2}, \quad v_{i+1/2,j,-1/2} = v_{i+1/2,j,1/2}, \\ &\rho_{i+1/2,j+1/2,-1} = \rho_{i+1/2,j+1/2,1}, \end{aligned} \tag{3.13}$$

using a similar argument as in (3.12).

3.1. Boundary condition for surface pressure p_s. The derived boundary condition (1.12) is needed to solve the surface pressure Poisson equation (3.9). As assumed earlier, in the case that $\mathcal{M}_0 = [0,1]^2$, we concentrate on the left boundary $x = 0$ for simplicity of presentation. The other three boundary sections $x = 1$, $y = 0, 1$ can be dealt with in the same manner. In PDE formulation, on the left boundary section $x = 0$, (1.12) indicates that

$$\frac{\partial p_s}{\partial x} = \nu_1 \, Ro \, \triangle \overline{u} = \nu_1 \, Ro \, \partial_x^2 \overline{u}, \tag{3.14}$$

where the second step is based on the fact that the velocity u vanishes; henceforth $\overline{u}$ vanishes on the boundary, too. The MAC mesh grid near the left boundary is shown in Figure 3.1.

Our methodology for approximating $\partial_x^2 \overline{u}$ as in (3.14) follows the approach taken by numerical methods for the 2-D NSE formulated in the vorticity-stream function, as given in (1.15), (1.16), based on local vorticity boundary conditions. The earliest work in this direction is due to Thom [27]. The more recent works [6], [10], [28] revived interest in the use of local formulae for vorticity on the boundary and analyzed the stability and convergence of a class of such formulae. The key point in these approaches is to convert the Neumann boundary condition for the stream function ψ, which states the no-slip velocity boundary condition, into a local vorticity boundary condition, such as Thom's formula.

A similar idea can be used in the approximation to $\partial_x^2 \overline{u}$ as in (3.14). In our scheme, the mean divergence-free boundary condition for the horizontal velocity, $(\nabla \cdot \boldsymbol{v}) \mid_{\partial \mathcal{M}_0} = 0$, can be converted into an approximation of the Neumann boundary condition for the surface pressure as derived in (1.12). In more detail, the following finite-difference method is applied on the boundary grid point $(0, j \pm 1/2)$:

$$\begin{aligned} \partial_x^2 \overline{u}_{0,j+1/2} &= \frac{\overline{u}_{-1,j+1/2} - 2\overline{u}_{0,j+1/2} + \overline{u}_{1,j+1/2}}{\triangle x^2} + O(h^2) \\ &= \frac{\overline{u}_{-1,j+1/2} + \overline{u}_{1,j+1/2}}{\triangle x^2} + O(h^2), \end{aligned} \tag{3.15}$$

where the second step is based on the fact that the velocity field $\boldsymbol{v}$ vanishes on the boundary. The second-order approximation (5.15) requires a value for $\overline{u}$ at grid point $(-1, j+1/2)$, which is a "ghost" point outside the computational domain. A consistent prescription of the value for $\overline{u}_{-1,j+1/2}$ relies on a second order centered difference of the mean divergence-free boundary condition $\overline{\nabla \cdot \boldsymbol{v}} \mid_{x=0} = 0$,

$$0 = (\partial_x \overline{u} + \partial_y \overline{v}) \mid_{x=0} = 0 + \partial_y \overline{v} \mid_{x=0} = \frac{\overline{u}_{1,j+1/2} - \overline{u}_{-1,j+1/2}}{2\triangle x} + O(h^2), \tag{3.16}$$

where the second step is due to the boundary condition $\overline{v} = 0$ on $\partial\mathcal{M}_0$. The finite-difference identity (3.16) directs us to take

$$\overline{u}_{-1,j+1/2} = \overline{u}_{1,j+1/2}, \tag{3.17}$$

whose substitution into (3.15), (3.14) gives a second order approximation of the derived Neumann boundary condition (1.12),

$$\frac{\partial p_s}{\partial \boldsymbol{n}} \mid_{0,y_{j+1/2}} = \frac{\partial p_s}{\partial x} \mid_{0,y_{j+1/2}} = Ro\, \frac{2\nu_1}{\triangle x^2}\overline{u}_{1,j+1/2}. \qquad \text{(ASPBC)} \tag{3.18}$$

The evaluation of $\frac{\partial p_s}{\partial \boldsymbol{n}}$ at three other boundary sections can be derived in the same fashion. We refer to the above formula as the accurate surface pressure boundary condition (ASPBC). A similar derivation for the local pressure boundary condition in the spatially discrete level of the incompressible NSE can be found in a recent paper of Johnston and Liu [11]. Therefore, we have the following set of boundary conditions for p_s in the discrete version:

$$\begin{aligned} (p_s)_{-1/2,j+1/2} &= (p_s)_{1/2,j+1/2} - Ro\, \frac{2\nu_1}{\triangle x}\overline{u}_{1,j+1/2}, \\ (p_s)_{i+1/2,-1/2} &= (p_s)_{i+1/2,1/2} - Ro\, \frac{2\nu_1}{\triangle y}\overline{v}_{i+1/2,1}. \end{aligned} \tag{3.19}$$

3.2. The MAC scheme for the PEs. Thus the system of MAC spatial discretization of the PEs can be written as

$$\begin{cases} u_t + \mathcal{N}_h(\boldsymbol{u}, u) + \dfrac{1}{Ro}\Big(-f\overline{\overline{v}} + \mathcal{P}NRX + D_x p_s\Big) = L_{1,h}u \quad \text{at} \ \triangle, \\ v_t + \mathcal{N}_h(\boldsymbol{u}, v) + \dfrac{1}{Ro}\Big(f\overline{\overline{u}} + \mathcal{P}NRY + D_y p_s\Big) = L_{1,h}v \quad \text{at} \ \bigcirc, \\ D_z\boldsymbol{v} \mid_{z=-H_0} = 0, \quad D_z\boldsymbol{v} \mid_{z=0} = \dfrac{\tau_0}{\nu_2}, \\ \boldsymbol{v}\cdot\boldsymbol{n} = 0, \quad \boldsymbol{v}\cdot\tau = 0 \quad \text{on} \ \partial\mathcal{M}_0 \times [-H_0, 0], \end{cases} \tag{3.20a}$$

$$\begin{cases} (\triangle_h p_s)_{i+1/2,j+1/2} = Ro\,\overline{\mathcal{F}P}_{i+1,j+1/2}, \\ \dfrac{\partial p_s}{\partial \boldsymbol{n}} = Ro\,\nu_1\,(\triangle_h \boldsymbol{v})\cdot\boldsymbol{n}, \end{cases} \tag{3.20b}$$

$$w_{i+1/2,j+1/2,k} = -\triangle z \sum_{l=0}^{k-1}\Big((D_x u)_{i+1/2,j+1/2,l+1/2} + (D_y v)_{i+1/2,j+1/2,l+1/2}\Big), \tag{3.20c}$$

$$\begin{cases} \rho_t + \mathcal{N}_h(\boldsymbol{u}, \rho) = L_{2,h}\rho \quad \text{at} \ \ (i+1/2, j+1/2, k), \\ \tilde{D}_z\rho \mid_{z=0} = \dfrac{\rho_f}{\kappa_2}, \quad \tilde{D}_z\rho \mid_{z=-H_0} = 0, \\ \dfrac{\partial \rho}{\partial \boldsymbol{n}} = 0 \quad \text{on} \ \partial\mathcal{M}_0 \times [-H_0, 0]. \end{cases} \tag{3.20d}$$

Hereafter we denote $L_{1,h} = (\nu_1\triangle_h + \nu_2 D_z^2)$, $L_{2,h} = (\kappa_1\triangle_h + \kappa_2 D_z^2)$ for simplicity of presentation.

3.3. Mean divergence-free property. In this section, we argue that the numerical velocity field $\boldsymbol{v}_h$, the solution of the system (3.20), has free mean-divergence in a discrete level; i.e.,

$$D_x\overline{u} + D_y\overline{v} = 0 \quad \text{on mesh point} \quad (i+1/2, j+1/2), \tag{3.21}$$

where $\overline{u}$, $\overline{v}$ are defined in the same way as in (3.10). To see this, we use a similar argument as in (1.14a), (1.14b), and (1.14c). Taking the discrete divergence of the two momentum equations in (3.20a) at mesh points $(i+1/2, j+1/2, k+1/2)$, summing in the z-direction, and keeping in mind the discrete Poisson equation for p_s as in (3.8), (3.9), we have

$$(\overline{\nabla_h \cdot \boldsymbol{v}})_t = \nu_1 \triangle_h \overline{\nabla_h \cdot \boldsymbol{v}} \quad \text{at} \quad (i+1/2, j+1/2). \tag{3.22}$$

In the derivation of (3.22), we used the fact that the composition of discrete divergence and discrete gradient (D_x, D_y) gives exactly the five-point Laplacian in the context of the MAC spatial discretization. Another important fact we used in the derivation of (3.22) is that, on MAC grids, the Laplacian operator $\triangle_h$ and the divergence operator are commutative. These two points represents a crucial advantage of the MAC grid.

The homogeneous initial data for $\overline{\nabla_h \cdot \boldsymbol{v}}$ is obvious:

$$\Big((\overline{\nabla_h \cdot \boldsymbol{v}})(\cdot, t=0)\Big)_{i+1/2, j+1/2} = 0. \tag{3.23}$$

It remains to make sure it vanishes on the lateral boundary $\partial\mathcal{M}_0$. We concentrate on the boundary section $x = 0$. The discrete divergence of $\overline{\boldsymbol{v}}$ on $x = 0$ can be evaluated as

$$\begin{aligned}
(\overline{\nabla_h \cdot \boldsymbol{v}})_{0,j+1/2} &= \frac{1}{2}\Big((\overline{\nabla_h \cdot \boldsymbol{v}})_{-1/2,j+1/2} + (\overline{\nabla_h \cdot \boldsymbol{v}})_{1/2,j+1/2}\Big) \\
&= \frac{1}{2}\Big(\frac{\overline{u}_{0,j+1/2} - \overline{u}_{-1,j+1/2}}{\triangle x} + \frac{\overline{v}_{-1/2,j+1} - \overline{v}_{-1/2,j}}{\triangle y} \\
&\qquad + \frac{\overline{u}_{1,j+1/2} - \overline{u}_{0,j+1/2}}{\triangle x} + \frac{\overline{v}_{1/2,j+1} - \overline{v}_{1/2,j}}{\triangle y}\Big), \\
&= \frac{\overline{u}_{1,j+1/2} - \overline{u}_{-1,j+1/2}}{2\triangle x} + \frac{1}{2}\Big(\frac{\overline{v}_{-1/2,j+1} - \overline{v}_{-1/2,j}}{\triangle y} + \frac{\overline{v}_{1/2,j+1} - \overline{v}_{1/2,j}}{\triangle y}\Big),
\end{aligned} \tag{3.24}$$

where $\overline{u}_{-1,j+1/2}$, $\overline{v}_{-1/2,j}$ are "ghost" point computational values for $\overline{u}$, $\overline{v}$. Meanwhile, the reflection rule (3.11) (due to the no-slip boundary condition for v) gives that the last two terms in (3.12) vanish, i.e.,

$$(\overline{\nabla_h \cdot \boldsymbol{v}})_{0,j+1/2} = \frac{\overline{u}_{1,j+1/2} - \overline{u}_{-1,j+1/2}}{2\triangle x}. \tag{3.25}$$

By the identity (3.17) that $\overline{u}_{-1,j+1/2} = \overline{u}_{1,j+1/2}$, which is used for the derivation of the Neumann boundary condition for the surface pressure p_s, we conclude that the mean discrete divergence of $\boldsymbol{v}$ vanishes on the boundary $x = 0$. In other words, the ASPBC (3.18) conversely indicates the choice for $\overline{u}_{-1,j+1/2}$ as in (3.17). The substitution of (3.17) into (3.25) gives

$$(\overline{\nabla_h \cdot \boldsymbol{v}})_{0,j+1/2} = 0. \tag{3.26}$$

The combination of (3.26), (3.22), (3.23) indicates (3.21), which states that the numerical solution $\boldsymbol{v}_h$ of the system (3.20) has exactly zero discrete mean-divergence. Henceforth, the formula (3.20c) for the determination of vertical velocity is consistent with the combination of divergence-free property of the numerical velocity $\boldsymbol{u}_h$:

$$\nabla_h \cdot \boldsymbol{v}_h + D_z w = 0, \tag{3.27}$$

and the boundary condition for the vertical velocity w at $z = 0$ and $z = -H_0$:

$$w_{i+1/2,j+1/2,0} = w_{i+1/2,j+1/2,N} = 0. \tag{3.28}$$

4. Convergence analysis of the fully discretized scheme using the backward Euler method combined with the MAC grid. The MAC spatial discretization can be easily implemented in practical computations, combined with either backward Euler or Crank–Nicolson schemes as outlined in section 2. For technical simplicity, the periodic boundary condition is assumed in the horizontal (x, y)-plane so that only the top and bottom boundary sections need to be taken into consideration in the convergence analysis below. The scheme with physical lateral boundary conditions can be dealt with in a similar fashion, with more technical details involved in the consistency analysis. We skip it for the sake of brevity.

The fully discretized scheme using backward Euler temporal discretization is formulated as below. The corresponding Crank–Nicolson method can be similarly proposed and analyzed. We omit it in this article.

$$\begin{cases} \dfrac{u^{n+1} - u^n}{\triangle t} + \mathcal{N}_h(\boldsymbol{u}^n, u^n) + \dfrac{1}{Ro}\Big(-f\overline{\overline{v}}^n + \mathcal{P}NRX^n + D_x p_s^n\Big) \\ \qquad = L_{1,h} u^{n+1} \quad \text{at} \ \triangle, \\ \dfrac{v^{n+1} - v^n}{\triangle t} + \mathcal{N}_h(\boldsymbol{u}^n, v^n) + \dfrac{1}{Ro}\Big(f\overline{\overline{u}}^n + \mathcal{P}NRY^n + D_y p_s^n\Big) \\ \qquad = L_{1,h} v^{n+1} \quad \text{at} \ \bigcirc, \\ D_z \boldsymbol{v} \mid_{z=-H_0} = 0, \quad D_z \boldsymbol{v} \mid_{z=0} = 0, \end{cases} \tag{4.1a}$$

$$(\triangle_h p_s)^{n+1}_{i+1/2,j+1/2} = Ro\, \overline{\mathcal{F}P}^{n+1}_{i+1,j+1/2}, \tag{4.1b}$$

$$w^{n+1}_{i+1/2,j+1/2,k} = -\triangle z \sum_{l=0}^{k-1} \Big((D_x u)^{n+1}_{i+1/2,j+1/2,l+1/2} + (D_y v)^{n+1}_{i+1/2,j+1/2,l+1/2} \Big), \tag{4.1c}$$

$$\begin{cases} \dfrac{\rho^{n+1} - \rho^n}{\triangle t} + \mathcal{N}_h(\boldsymbol{u}^n, \rho^n) = L_{2,h} \rho^{n+1} \quad \text{at} \ \bullet, \\ \tilde{D}_z \rho \mid_{z=0} = 0, \quad \tilde{D}_z \rho \mid_{z=-H_0} = 0. \end{cases} \tag{4.1d}$$

4.1. Main theorem and some notations. The following notations of L^2 norms in a discrete level need to be introduced.

Notation 4.1. For any pair of variables u^a, u^b which are defined at the mesh points $(i, j+1/2, k+1/2)$ (such as u, $\tilde{D}_x u$, $\tilde{D}_y u$, $\tilde{D}_z u$, etc.), the discrete L^2-inner product is given by

$$\langle u^a, u^b\rangle_1 = \sum_{k=0}^{N-1}\sum_{j=0}^{N-1}\sum_{i=0}^{N-1} u^a_{i,j+1/2,k+1/2}\, u^b_{i,j+1/2,k+1/2}\, h^3. \tag{4.2a}$$

For any pair of variables v^a, v^b which are defined at the mesh points $(i+1/2, j, k+1/2)$ (such as v, $\tilde{D}_x v$, $\tilde{D}_y v$, $\tilde{D}_z v$, etc.), the discrete L^2-inner product is given by

$$\langle v^a, v^b\rangle_2 = \sum_{k=0}^{N-1}\sum_{j=0}^{N-1}\sum_{i=0}^{N-1} v^a_{i+1/2,j,k+1/2}\, v^b_{i+1/2,j,k+1/2}\, h^3. \tag{4.2b}$$

For any pair of variables ρ^a, ρ^b defined at the mesh points $(i+1/2, j+1/2, k)$ (such as ρ, w, $\tilde{D}_x\rho$, $\tilde{D}_y\rho$, $\tilde{D}_z\rho$, etc.), the discrete L^2-inner product is given by

$$\begin{aligned}\langle \rho^a, \rho^b\rangle_3 = \sum_{j=0}^{N-1}\sum_{i=0}^{N-1}\Big(&\sum_{k=1}^{N-1} \rho^a_{i+1/2,j+1/2,k}\,\rho^b_{i+1/2,j+1/2,k} \\ &+ \frac{1}{2}\rho^a_{i+1/2,j+1/2,0}\,\rho^b_{i+1/2,j+1/2,0} + \frac{1}{2}\rho^a_{i+1/2,j+1/2,N}\,\rho^b_{i+1/2,j+1/2,N}\Big)\, h^3.\end{aligned} \tag{4.2c}$$

Finally, for any pair of variables p^a, p^b defined at the mesh points $(i+1/2, j+1/2, k+1/2)$ (such as p, $D_x u$, $D_y v$, $D_z w$), the discrete L^2-inner product is defined by

$$\langle p^a, p^b\rangle_4 = \sum_{k=0}^{N-1}\sum_{j=0}^{N-1}\sum_{i=0}^{N-1} p^a_{i+1/2,j+1/2,k+1/2}\, p^b_{i+1/2,j+1/2,k+1/2}\, h^3. \tag{4.2d}$$

Clearly, all the discrete L^2-inner products defined above are second order accurate. The corresponding L^2_h norms can be defined accordingly. In addition, we set a vector norm for the horizontal velocity as $\|\boldsymbol{v}\|^2_{\boldsymbol{L}^2_h} = \|u\|^2_1 + \|v\|^2_2$, where $\|u\|^2_1 = \langle u, u\rangle_1$, $\|v\|^2_2 = \langle v, v\rangle_2$.

The following is the main theorem of this paper.

THEOREM 4.1. *Let $\boldsymbol{u}_e = (\boldsymbol{v}_e, w_e)$, p_e, ρ_e be the exact solution of the PEs* (1.1), (1.2), *with periodic boundary condition in the horizontal (x, y)-plane, and let $(\boldsymbol{v}_{\triangle t,h}, w_{\triangle t,h}, \rho_{\triangle t,h})$ be the numerical solution of the backward Euler coupled with the MAC grid in* (4.1). *We assume that $\triangle t \le Ch$, in which C is an arbitrary fixed constant. Then the following convergence result holds as $\triangle t$ and h go to zero:*

$$\|\boldsymbol{v}_e - \boldsymbol{v}_{\triangle t,h}\|_{L^\infty(0,T;\boldsymbol{L}^2_h)} + \|\rho_e - \rho_{\triangle t,h}\|_{L^\infty(0,T;L^2_h)} \le C(\triangle t + h^2), \tag{4.3a}$$

where the constant C depends only on the regularity of the exact solution

$$C = C\Big(\|\boldsymbol{u}_e\|_{L^\infty(0,T;C^{7,\alpha})}, \|\rho_e\|_{L^\infty(0,T;C^{7,\alpha})}, \|\boldsymbol{u}_e\|_{C^4(0,T;C^{2,\alpha})}, \|\rho_e\|_{C^4(0,T;C^{2,\alpha})}\Big). \tag{4.3b}$$

The rest of the paper is devoted to the proof of Theorem 4.1. The main steps include the following: 1. The numerical horizontal velocity is shown to have vanishing averaged divergence. 2. The leading order consistency analysis, which gives a construction of approximate velocity and density profiles satisfying the numerical scheme up to an $O(\triangle t + h^2)$ error. Moreover, the constructed horizontal velocity satisfies zero mean-divergence property at the discrete level. 3. Higher order expansion, up to $O(\triangle t^3 + h^4)$ expansion, of the numerical scheme. That makes the recovery of the L^∞ a priori assumption possible, for both the horizontal and the vertical velocity fields in the full nonlinear system of the PEs, by the usage of inverse inequalities. 4. The energy estimate for the error functions. The four steps will be presented in sections 4.2–4.5 below, respectively.

4.2. Evolution for the mean divergence of $\boldsymbol{v}$. To facilitate the proof of Theorem 4.1, we show that the calculated horizontal velocity at each time step has free mean-divergence at the discrete level; i.e., (3.21) is satisfied for $\boldsymbol{v}$ at each time step. The argument is similar to the one in section 3.3. Taking the discrete divergence of the momentum equations in (4.1a) at mesh points $(i + 1/2, j + 1/2, k + 1/2)$ and summing in the z-direction gives

$$\frac{\overline{\nabla_h \cdot \boldsymbol{v}^{n+1}} - \overline{\nabla_h \cdot \boldsymbol{v}^n}}{\triangle t} = \nu_1 \triangle_h (\overline{\nabla_h \cdot \boldsymbol{v}^{n+1}}) \quad \text{at} \quad (i + 1/2, j + 1/2), \tag{4.4a}$$

since all other terms at the time step t^n were canceled by the surface pressure Poisson equation (4.1b) at the same time step. The combination of the evolution equation in (4.4a) and the homogeneous initial data,

$$\overline{\nabla_h \cdot \boldsymbol{v}^0} = 0, \tag{4.4b}$$

shows that the numerical solution $\boldsymbol{v}_{h,\triangle t}$ of the scheme (4.1) has exactly zero discrete mean-divergence. As a result, the combined system (3.27), (3.28) is valid for $\boldsymbol{v}^n$, w^n at any time step t^n.

Furthermore, the numerical scheme (4.1a) for the momentum equation and the discrete Poisson equation (4.1b) can also be reformulated in a form similar to that of (1.5), (1.6) in the PDE level, for the sake of simplicity of the convergence analysis given below. We denote the total pressure variable p at mesh points $(i+1/2, j+1/2, k+1/2)$ as

$$p_{i+1/2,j+1/2,k+1/2} = \mathcal{P}R_{i+1/2,j+1/2,k+1/2} + (p_s)_{i+1/2,j+1/2}, \tag{4.5a}$$

where $\mathcal{P}R$, a discrete realization of $\int_z^0 \rho(x, y, s)\, ds$, is defined in a similar way as in (3.7):

$$\begin{aligned} \mathcal{P}R_{i+1/2,j+1/2,N-1/2} &= \frac{1}{2} \triangle z\, \rho_{i+1/2,j+1/2,N}, \\ \mathcal{P}R_{i+1/2,j+1/2,k-1/2} &= \mathcal{P}R_{i+1/2,j,k+1/2} + \triangle z\, \rho_{i+1/2,j+1/2,k}. \end{aligned} \tag{4.5b}$$

Clearly, (4.5) is a discrete version of the hydrostatic equation. One obvious fact is that

$$D_z p = \rho \qquad \text{at the mesh point } (i + 1/2, j + 1/2, k). \tag{4.6}$$

Therefore the scheme (4.1) can be rewritten as the following system:

$$\text{(4.7a)}\quad \begin{cases} \dfrac{u^{n+1}-u^n}{\triangle t}+\mathcal{N}_h(\boldsymbol{u}^n,u^n)+\dfrac{1}{Ro}\Big(-f\overline{\overline{v}}^n+D_xp^n\Big)=L_{1,h}u^{n+1} \quad \text{at} \ \triangle, \\ \dfrac{v^{n+1}-v^n}{\triangle t}+\mathcal{N}_h(\boldsymbol{u}^n,v^n)+\dfrac{1}{Ro}\Big(f\overline{\overline{u}}^n+D_yp^n\Big)=L_{1,h}v^{n+1} \quad \text{at} \ \bigcirc, \\ D_z\boldsymbol{v}^{n+1}\mid_{z=-H_0}=0, \quad D_z\boldsymbol{v}^{n+1}\mid_{z=0}=0, \end{cases}$$

$$\text{(4.7b)}\qquad D_zp^{n+1}=\rho^{n+1} \quad \text{at} \ \ (i+1/2,j+1/2,k),$$

$$\text{(4.7c)}\qquad \begin{cases} \nabla_h\cdot\boldsymbol{v}^{n+1}+D_zw^{n+1}=0, \\ w^{n+1}_{i+1/2,j+1/2,0}=w^{n+1}_{i+1/2,j+1/2,N}=0, \end{cases}$$

$$\text{(4.7d)}\qquad \begin{cases} \dfrac{\rho^{n+1}-\rho^n}{\triangle t}+\mathcal{N}_h(\boldsymbol{u}^n,\rho^n)=L_{2,h}\rho^{n+1} \quad \text{at} \ \bullet, \\ \tilde{D}_z\rho\mid_{z=0}=0, \quad \tilde{D}_z\rho\mid_{z=-H_0}=0. \end{cases}$$

We remark that the mean divergence-free property for the numerical horizontal velocity field and the corresponding identities (3.27), (3.28) assure that the 3-D velocity field is orthogonal to the horizontal and vertical gradients of the total pressure field p in the staggered L^2 space introduced in (4.2), i.e.,

$$\text{(4.8)}\qquad \langle u,D_xp\rangle_1+\langle v,D_yp\rangle_2+\langle w,D_zp\rangle_3=-\langle(\nabla_h\cdot\boldsymbol{v}+D_zw),p\rangle_4=0,$$

by usage of summing by parts in the MAC grid and of the boundary condition for the velocity field. This crucial point makes possible the convergence analysis of the whole numerical scheme using the MAC spatial discretization.

4.3. Leading order consistency analysis. Our goal is to construct approximate velocity profiles $\boldsymbol{V}^0=(U^0,V^0)$, $\boldsymbol{W}^0$ and approximate density profile Θ^0, and to show that their combination with exact pressure profile p_e satisfies the numerical scheme (4.7) up to an $O(\triangle t+h^2)$ error. Furthermore, the constructed $\boldsymbol{V}^0$ has to be assured to have zero mean-divergence in the discrete sense, i.e.,

$$\text{(4.9)}\qquad \overline{\nabla_h\cdot\boldsymbol{V}^0}=0 \quad \text{at} \quad (i+1/2,j+1/2),$$

so that the vertical velocity $\boldsymbol{W}^0$ can be determined by the formula in the same way as in (4.7c) consistent with its boundary condition:

$$\text{(4.10)}\qquad \boldsymbol{W}^0_{i+1/2,j+1/2,k}=-\triangle z\sum_{l=0}^{k-1}\Big((D_xU^0)_{i+1/2,j+1/2,l}+(D_yV^0)_{i+1/2,j+1/2,l}\Big).$$

In other words, the combination of (4.9) and (4.10) gives

$$\text{(4.11)}\qquad \begin{cases} \nabla_h\cdot\boldsymbol{V}^0+D_zW^0=0, \\ \boldsymbol{W}^0_{i+1/2,j+1/2,0}=\boldsymbol{W}^0_{i+1/2,j+1/2,N}=0, \end{cases}$$

which is analogous to (4.7c).

The construction of the leading term for the horizontal velocity field $\boldsymbol{V}^0$ relies on the fact that any C^1 function g in $\mathcal{M}$ can be uniquely recovered from its average in the z-direction and its derivative with respect to z by

$$g(x,y,z) = \int_{-H_0}^{z} g_z(x,y,s)\,ds + \overline{g}(x,y) - \frac{1}{H_0}\int_{-H_0}^{0}\int_{-H_0}^{z'} g_z(x,y,s)\,ds\,dz'. \tag{4.12}$$

As a result, the exact horizontal velocity field $\boldsymbol{v}_e$ can be represented as

$$\begin{aligned} u_e(x,y,z) &= \int_{-H_0}^{z} \partial_z u_e(x,y,s)\,ds + \overline{u_e}(x,y) - \frac{1}{H_0}\int_{-H_0}^{0}\int_{-H_0}^{z} \partial_z u_e(x,y,s)\,ds\,dz, \\ v_e(x,y,z) &= \int_{-H_0}^{z} \partial_z v_e(x,y,s)\,ds + \overline{v_e}(x,y) - \frac{1}{H_0}\int_{-H_0}^{0}\int_{-H_0}^{z} \partial_z v_e(x,y,s)\,ds\,dz. \end{aligned} \tag{4.13}$$

The discrete form of the recovery formula (4.13) applied to U^0, V^0 can be written as follows:

$$\begin{aligned} U^0_{i,j+1/2,k+1/2} &= -\mathcal{P}UZ^0_{i,j+1/2,k+1/2} + \overline{U^0}_{i,j+1/2} + \overline{\mathcal{P}UZ}^0_{i,j+1/2}, \\ V^0_{i+1/2,j,k+1/2} &= -\mathcal{P}VZ^0_{i+1/2,j,k+1/2} + \overline{V^0}_{i+1/2,j} + \overline{\mathcal{P}VZ}^0_{i+1/2,j}, \end{aligned} \tag{4.14}$$

the construction of the mean velocity field $\overline{U}^0$, $\overline{V}^0$ will be given later, and $\mathcal{P}UZ^0$, $\mathcal{P}VZ^0$ represents the discrete integral of $\partial_z u_e$, $\partial_z v_e$ from $-H_0$ up to $z_k = (k+\frac{1}{2})\triangle z$, respectively. Keeping in mind that $\partial_z u_e$, $\partial_z v_e$ are defined on the numerical grids $(i, j \pm 1/2, k)$, $(i \pm 1/2, j, k)$, respectively, we express such integrals as

$$\begin{aligned} \mathcal{P}UZ^0_{i,j+1/2,-1/2} &= -\frac{1}{2}\triangle z\,(\partial_z u_e)_{i,j+1/2,0}, \\ \mathcal{P}UZ^0_{i,j+1/2,k+1/2} &= \mathcal{P}UZ^0_{i,j+1/2,k-1/2} + \triangle z\,(\partial_z u_e)_{i,j+1/2,k}, \end{aligned} \tag{4.15a}$$

$$\begin{aligned} \mathcal{P}VZ^0_{i+1/2,j,-1/2} &= -\frac{1}{2}\triangle z\,(\partial_z v_e)_{i+1/2,j,0}, \\ \mathcal{P}VZ^0_{i+1/2,j,k+1/2} &= \mathcal{P}VZ^0_{i+1/2,j,k-1/2} + \triangle z\,(\partial_z v_e)_{i+1/2,j,k}. \end{aligned} \tag{4.15b}$$

Obviously, the combination of (4.14) and (4.15) gives

$$\begin{aligned} &\sum_{k=0}^{N_z-1} (\triangle z\, U^0_{i,j+1/2,k+1/2}) = \overline{U^0}_{i,j+1/2}, \quad (D_z U^0)_{i,j+1/2,k} = (\partial_z u_e)_{i,j+1/2,k}, \\ &\sum_{k=0}^{N_z-1} (\triangle z\, V^0_{i+1/2,j,k+1/2}) = \overline{V^0}_{i+1/2,j}, \quad (D_z V^0)_{i+1/2,j,k} = (\partial_z v_e)_{i+1/2,j,k}. \end{aligned} \tag{4.16}$$

We use the "mean stream function" corresponding to the exact velocity solution $\boldsymbol{v}_e$ to construct the mean velocity field $\overline{\boldsymbol{V}^0}$ appearing in the construction formula (4.14). Since the average of the exact velocity field $\overline{\boldsymbol{v}_e}$ is divergence-free in the 2-D domain $\mathcal{M}_0$, as shown in (1.4), there exists a mean stream function $\overline{\psi_e}$ such that

$$\overline{\boldsymbol{v}_e} = \nabla^{\perp}\overline{\psi_e} = (-\partial_y\overline{\psi_e}, \partial_x\overline{\psi_e}). \tag{4.17}$$

Subsequently, the average of $\boldsymbol{V}^0$ (in the z-direction) can be determined via second order finite-difference of the exact "mean stream function"

$$\begin{aligned}\overline{U^0} &= -D_y\overline{\psi_e} = -\frac{\overline{\psi_e}_{i,j+1} - \overline{\psi_e}_{i,j}}{\triangle y} \quad \text{at} \quad (i, j+1/2),\\ \overline{V^0} &= D_x\overline{\psi_e} = \frac{\overline{\psi_e}_{i+1,j} - \overline{\psi_e}_{i,j}}{\triangle x} \quad \text{at} \quad (i+1/2, j).\end{aligned} \tag{4.18}$$

It should be remarked that the mean stream function is evaluated at regular mesh points (i, j), $0 \le i, j \le N$. Obviously, (4.18) gives

$$D_x\overline{U^0} + D_y\overline{V^0} = -D_x(D_y\overline{\psi_e}) + D_y(D_x\overline{\psi_e}) = 0, \tag{4.19}$$

which along with the identity (4.16) assures that the mean divergence-free property is automatically satisfied for the constructed leading velocity field

$$\overline{\nabla_h \cdot \boldsymbol{V}^0} = 0 \quad \text{at} \quad (i+1/2, j+1/2). \tag{4.20}$$

Accordingly, the recovery formula analogous to (4.2) is used to construct the leading vertical velocity

$$\boldsymbol{W}^0_{i+1/2,j+1/2,k} = -\triangle z \sum_{l=0}^{k-1}\Big((D_xU^0)_{i+1/2,j+1/2,l+1/2} + (D_yV^0)_{i+1/2,j+1/2,l+1/2}\Big), \tag{4.21}$$

which is compatible with the boundary condition $\boldsymbol{W}^0_{i+1/2,j+1/2,0} = \boldsymbol{W}^0_{i+1/2,j+1/2,N} = 0$.

The proposition below states that the constructed leading velocity profile, together with its temporal derivative, is within $O(h^2)$ difference with the exact velocity $\boldsymbol{u}_e = (\boldsymbol{v}_e, w_e)$. Its verification is omitted in this paper for brevity and will appear elsewhere.

PROPOSITION 4.2. *The following estimates for $\boldsymbol{V}^0$, $\boldsymbol{W}^0$ hold:*

$$\|\boldsymbol{V}^0 - \boldsymbol{v}_e\|_{W^{m,\infty}(\mathcal{M})} \le Ch^2\|\boldsymbol{v}_e\|_{C^{m+3}} \quad \textit{for} \;\; m = 0, 1, 2\ldots, \tag{4.22a}$$

$$\|W^0 - w_e\|_{W^{m,\infty}(\mathcal{M})} \le Ch^2\|\boldsymbol{v}_e\|_{C^{m+4}}. \tag{4.22b}$$

Here $\|\cdot\|_{W^{m,\infty}(\mathcal{M})}$ represents the maximum value at the corresponding mesh points of the given function up to mth order finite-difference over the 3-D domain $\mathcal{M}$. Furthermore, the difference between the time derivatives of $\boldsymbol{V}^0$ and $\boldsymbol{v}_e$ can be controlled by

$$\partial_t^m\boldsymbol{V}^0 = \partial_t^m\boldsymbol{v}_e + O(h^2)\|\partial_t^m\boldsymbol{v}_e\|_{C^3} \quad \textit{for} \;\; m \ge 1. \tag{4.23}$$

In addition, we observe that $\boldsymbol{V}^0$ exactly satisfies the boundary condition in the discrete form as given in (4.7) at the top $z = 0$ and at the bottom $z = -H_0$:

$$\begin{aligned}&(D_zU^0)_{i,j+1/2,0} = 0, \quad (D_zV^0)_{i+1/2,j,0} = 0,\\ &(D_zU^0)_{i,j+1/2,N} = 0, \quad (D_zV^0)_{i+1/2,j,N} = 0,\end{aligned} \tag{4.24}$$

due to its construction in (4.15) and the fact that $\partial_z \boldsymbol{v}_e = 0$ at the two boundary sections.

The leading order density profile is composed of the exact density and a correction term

$$\Theta^0 = \rho_e + h^2 \Theta^1. \tag{4.25}$$

The addition of the $O(h^2)$ correction terms $h^2\Theta^1$ is due to the higher order consistency of the approximate profile Θ with the boundary condition given in the numerical scheme (4.7d), which is required in the error analysis presented later. The correction function Θ^1 is constructed as the solution of the Poisson equation with Neumann boundary condition

(4.26)
$$\begin{cases} \triangle \Theta^1 = C^1 \equiv \dfrac{1}{|\mathcal{M}|} \left(\displaystyle\int_{\mathcal{M}_0} \frac{1}{6} \partial_z^3 \rho_e(x,y,-H_0)\, d\boldsymbol{x} - \int_{\mathcal{M}_0} \frac{1}{6} \partial_z^3 \rho_e(x,y,0)\, d\boldsymbol{x} \right), \\ \partial_z \Theta^1(x,y,-H_0) = -\dfrac{1}{6}\, \partial_z^3 \rho_e(x,y,-H_0), \quad \partial_z \Theta^1(x,y,0) = -\dfrac{1}{6}\, \partial_z^3 \rho_e(x,y,0). \end{cases}$$

Note that the number C^1 (a function of time t) is chosen so that $\int_{\mathcal{M}} C^1\, d\boldsymbol{x}\, dz = \int_{\partial \mathcal{M}} \frac{\partial \Theta^1}{\partial \boldsymbol{n}}\, d\boldsymbol{n}$ to maintain the consistency. The Schauder's estimate applied to the Poisson equation (4.26) gives that

$$\|\Theta^1\|_{C^{m,\alpha}} \le \|\rho_e\|_{C^{m+2,\alpha}}, \quad \|\partial_t^k \Theta^1\|_{C^{m,\alpha}} \le \|\partial_t^k \rho_e\|_{C^{m+2,\alpha}} \qquad \text{for } \ m \ge 2. \tag{4.27}$$

The choice of the boundary condition for Θ^1 in (4.26) implies that the approximated density Θ as given in the expansion (4.25) satisfies the discrete boundary condition in (4.7d) to an $O(h^5)$ order. It can be seen by local Taylor expansion for the exact density field ρ_e around the bottom boundary that

(4.28)
$$(\rho_e)_{i+1/2,j+1/2,-1} = (\rho_e)_{i+1/2,j+1/2,1} - \frac{\triangle z^3}{3}\, \partial_z^3 \rho_e(x_{i+1/2}, y_{j+1/2}, -H_0) + O(h^5) \|\rho_e\|_{C^5},$$

in which the no-flux boundary condition is used. The insertion of the boundary condition given by (4.26) into the Taylor expansion of Θ^1, along with Schauder's estimate $\|\Theta_1\|_{C^2} \le C \|\rho_e\|_{C^{5,\alpha}}$ given by (4.27), leads to

(4.29)
$$\Theta^1_{i+1/2,j+1/2,-1} = \Theta^1_{i+1/2,j+1/2,1} + \frac{\triangle z}{3}\, \partial_z^3 \rho_e(x_{i+1/2}, y_{j+1/2}, -H_0) + O(h^3) \|\rho_e\|_{C^{5,\alpha}}.$$

The combination of (4.28) and (4.29) results in the following estimate for $\Theta^0 = \rho_e + h^2\Theta^1$:

$$\Theta^0_{i+1/2,j+1/2,-1} = \Theta^0_{i+1/2,j+1/2,1} + O(h^5) \|\rho_e\|_{C^{5,\alpha}}, \tag{4.30}$$

which proves our claim. The top boundary $z = 0$ can be dealt with in the same manner.

It is straightforward to verify the following local truncation estimates:

$$
\text{(4.31a)}\quad \begin{cases} \dfrac{(U^0)^{n+1}-(U^0)^n}{\triangle t}+\mathcal{N}_h((\boldsymbol{U}^0)^n,(U^0)^n)+\dfrac{1}{Ro}\Big(-f(\overline{\overline{V^0}})^n+D_x p_e^n\Big) \\ \qquad =L_{1,h}(U^0)^{n+1}+\triangle t E_{\triangle t}^{u(0),n}+h^2E_h^{u(0),n} \quad \text{at } \triangle, \\ \dfrac{(V^0)^{n+1}-(V^0)^n}{\triangle t}+\mathcal{N}_h((\boldsymbol{U}^0)^n,(V^0)^n)+\dfrac{1}{Ro}\Big(f(\overline{\overline{U^0}})^n+D_y p_e^n\Big) \\ \qquad =L_{1,h}(V^0)^{n+1}+\triangle t E_{\triangle t}^{v(0),n}+h^2E_h^{v(0),n} \quad \text{at } \bigcirc, \\ (U^0)_{i,j+1/2,-1/2}^{n+1}=(U^0)_{i,j+1/2,1/2}^{n+1}, \quad (V^0)_{i+1/2,j,-1/2}^{n+1}=(V^0)_{i+1/2,j,1/2}^{n+1}, \end{cases}
$$

$$
\text{(4.31b)}\qquad D_z p_e^{n+1}=(\Theta^0)^{n+1}+h^2E_h^{p(0),n} \quad \text{at } (i+1/2,j+1/2,k),
$$

$$
\text{(4.31c)}\qquad \begin{cases} \nabla_h\cdot(\boldsymbol{V}^0)^{n+1}+D_z(\boldsymbol{W}^0)^{n+1}=0, \\ (\boldsymbol{W}^0)_{i+1/2,j+1/2,0}^{n+1}=(\boldsymbol{W}^0)_{i+1/2,j+1/2,N}^{n+1}=0, \end{cases}
$$

$$
\text{(4.31d)}\qquad \begin{cases} \dfrac{(\Theta^0)^{n+1}-(\Theta^0)^n}{\triangle t}+\mathcal{N}_h((\boldsymbol{U}^0)^n,(\Theta^0)^n) \\ \qquad =L_{2,h}(\Theta^0)^{n+1}+(\triangle t+h^2)E^{\rho(0),n} \quad \text{at } \bullet, \\ (\Theta^0)_{i+1/2,j+1/2,-1}^{n+1}=(\Theta^0)_{i+1/2,j+1/2,1}^{n+1}+h^5\boldsymbol{e}_{\rho b}, \end{cases}
$$

via high order Taylor expansion of the constructed solution $\boldsymbol{V}^0$, W^0, Θ^0, along with the usage of Proposition 4.2. The local error terms satisfy

(4.32)

$$
\begin{aligned} &|E^{u(0)}|,|E^{v(0)}|\le C\Big(\|\partial_t\boldsymbol{v}_e\|_{C^2}+\|\partial_t^2\boldsymbol{v}_e\|_{C^2}+\|\boldsymbol{u}_e\|_{C^6}(1+\|\boldsymbol{u}_e\|_{C^3})+\|p_e\|_{C^4}\Big), \\ &|E^{p(0)}|\le C\|\rho_e\|_{C^2}, \quad |E^{\rho(0)}|\le C\Big(\|\partial_t\rho_e\|_{C^2}+\|\partial_t^2\rho_e\|_{C^2}+\|\rho_e\|_{C^5}(1+\|\boldsymbol{u}_e\|_{C^4})\Big). \end{aligned}
$$

4.4. Higher order expansion of the numerical scheme. The consistency analysis (4.31) is not enough to recover the L^∞ a priori estimates for the approximate velocity field in the full nonlinear system of the PEs. We need to construct further fields, $(\boldsymbol{V}_h^1,\boldsymbol{W}_h^1,\Theta_h^1,P_h^1)$, $(\boldsymbol{V}_{\triangle t}^1,\boldsymbol{W}_{\triangle t}^1,\Theta_{\triangle t}^1,P_{\triangle t}^1)$, $(\boldsymbol{V}_{\triangle t}^2,\boldsymbol{W}_{\triangle t}^2,\Theta_{\triangle t}^2,P_{\triangle t}^2)$, and to introduce, for the error analysis, the fields $\boldsymbol{V}$, $\boldsymbol{W}$, Θ, P defined by

$$
\text{(4.33)}\quad \begin{aligned} &\boldsymbol{V}=\boldsymbol{V}^0+h^2\boldsymbol{V}_h^1+\triangle t\boldsymbol{V}_{\triangle t}^1+\triangle t^2\boldsymbol{V}_{\triangle t}^2, \\ &\boldsymbol{W}=\boldsymbol{W}^0+h^2\boldsymbol{W}_h^1+\triangle t\boldsymbol{W}_{\triangle t}^1+\triangle t^2\boldsymbol{W}_{\triangle t}^2, \\ &\Theta=\Theta^0+h^2\Theta_h^1+\triangle t\Theta_{\triangle t}^1+\triangle t^2\Theta_{\triangle t}^2, \quad P=p_e+h^2P_h^1+\triangle tP_{\triangle t}^1+\triangle t^2P_{\triangle t}^2. \end{aligned}
$$

These new fields depend solely on $(\boldsymbol{V}^0,\boldsymbol{W}^0,\Theta^0,p_e)$, namely, on the exact solution. Their construction is straightforward but lengthy; we omit the details. The expanded

profiles satisfy the backward Euler scheme combined with the MAC grid up to order $O(\triangle t^3 + h^4)$:

(4.34a)
$$\begin{cases} \dfrac{U^{n+1}-U^n}{\triangle t} + \mathcal{N}_h(\boldsymbol{U}^n, U^n) + \dfrac{1}{Ro}\Big(-f\overline{\overline{V^n}} + D_x P^n\Big) \\ \qquad = L_{1,h}U^{n+1} + (\triangle t^3 + h^4)E^{u,n}, \\ \dfrac{V^{n+1}-V^n}{\triangle t} + \mathcal{N}_h(\boldsymbol{U}^n, V^n) + \dfrac{1}{Ro}\Big(f\overline{\overline{U^n}} + D_y P^n\Big) \\ \qquad = L_{1,h}V^{n+1} + (\triangle t^3 + h^4)E^{v,n}, \\ U^{n+1}_{i,j+1/2,-1/2} = U^{n+1}_{i,j+1/2,1/2} + h^5 \boldsymbol{e}_{ub}, \quad V^{n+1}_{i+1/2,j,-1/2} = V^{n+1}_{i+1/2,j,1/2} + h^5 \boldsymbol{e}_{ub}, \end{cases}$$

(4.34b)
$$D_z P^{n+1} = \Theta^{n+1} + h^4 E^{p,n},$$

(4.34c)
$$\begin{cases} \nabla_h \cdot \boldsymbol{V}^{n+1} + D_z \boldsymbol{W}^{n+1} = 0, \\ \boldsymbol{W}^{n+1}_{i+1/2,j+1/2,0} = \boldsymbol{W}^{n+1}_{i+1/2,j+1/2,N} = 0, \end{cases}$$

(4.34d)
$$\begin{cases} \dfrac{\Theta^{n+1}-\Theta^n}{\triangle t} + \mathcal{N}_h(\boldsymbol{U}^n, \Theta^n) = L_{2,h}\Theta^{n+1} + (\triangle t^3 + h^4)E^{\rho,n}, \\ \Theta^{n+1}_{i+1/2,j+1/2,-1} = \Theta^{n+1}_{i+1/2,j+1/2,1} + h^5 \boldsymbol{e}_{\rho b}, \end{cases}$$

in which the local truncation error and the boundary error terms are bounded in the L^∞ norm

(4.34e)
$$|E^u|, |E^v|, |E^p|, |E^\rho||\boldsymbol{e}_{ub}|, |\boldsymbol{e}_{vb}|, |\boldsymbol{e}_{\rho b}| \le \mathcal{C}^*,$$

with the constant $\mathcal{C}^*$ depending on the exact solution. This completes the consistency analysis.

Remark 4.3. As stated earlier, the purpose of the higher order expansion (4.33) is to obtain the L^∞ estimate of the error function via its L^2 norm in higher order accuracy by utilizing an inverse inequality in spatial discretization, which will be shown below. Such expansion is always possible under suitable regularity assumption of the exact solution. A detailed analysis shows that

(4.35)
$$|\boldsymbol{v}_e - \boldsymbol{V}| + |\boldsymbol{w}_e - \boldsymbol{W}| + |\rho_e - \Theta| \le C(\triangle t + h^2),$$

with C introduced in Theorem 4.1. This estimate will be used later.

Remark 4.4. We note that there is no $O(h^3)$ term in the higher order expansion (4.33). This is due to the centered difference we used in the spatial discretization, which gives local truncation errors with only even order, etc., $O(h^2)$, $O(h^4)$.

4.5. Proof of Theorem 4.1. We consider the following error functions:

(4.36)
$$\tilde{\boldsymbol{v}} = (\tilde{u}, \tilde{v}) = \boldsymbol{V} - \boldsymbol{v} = (U-u, V-v), \quad \tilde{w} = \boldsymbol{W} - w, \quad \tilde{p} = P - p, \quad \tilde{\rho} = \Theta - \rho.$$

Subtracting (4.7) from (4.34), we obtain the following system for the error functions:

(4.37a)
$$\begin{cases} \dfrac{\tilde{u}^{n+1}-\tilde{u}^n}{\triangle t}+\mathcal{E}NLU^n+\dfrac{1}{Ro}\Big(-f\overline{\tilde{v}}^n+D_x\tilde{p}^n\Big)=L_{1,h}\tilde{u}^{n+1}+(\triangle t^3+h^4)E^{u,n}, \\ \dfrac{\tilde{v}^{n+1}-\tilde{v}^n}{\triangle t}+\mathcal{E}NLV^n+\dfrac{1}{Ro}\Big(f\overline{\tilde{u}}^n+D_y\tilde{p}^n\Big)=L_{1,h}\tilde{v}^{n+1}+(\triangle t^3+h^4)E^{v,n}, \\ \tilde{u}^{n+1}_{i,j+1/2,-1/2}=\tilde{u}^{n+1}_{i,j+1/2,1/2}+h^5\boldsymbol{e}_{ub}, \quad \tilde{v}^{n+1}_{i+1/2,j,-1/2}=\tilde{v}^{n+1}_{i+1/2,j,1/2}+h^5\boldsymbol{e}_{ub}, \end{cases}$$

(4.37b)
$$D_z\tilde{p}^{n+1}=\tilde{\rho}^{n+1}+h^4E^{p,n},$$

(4.37c)
$$\begin{cases} \nabla_h\cdot\tilde{\boldsymbol{v}}^{n+1}+\tilde{D}_z\tilde{w}^{n+1}=0, \\ \tilde{w}^{n+1}_{i+1/2,j+1/2,0}=\tilde{w}^{n+1}_{i+1/2,j+1/2,N}=0, \end{cases}$$

(4.37d)
$$\begin{cases} \dfrac{\tilde{\rho}^{n+1}-\tilde{\rho}^n}{\triangle t}+\mathcal{E}NLR^n=L_{2,h}\tilde{\rho}^{n+1}+(\triangle t^3+h^4)E^{\rho,n}, \\ \tilde{\rho}^{n+1}_{i+1/2,j+1/2,-1}=\tilde{\rho}^{n+1}_{i+1/2,j+1/2,1}+h^5\boldsymbol{e}_{\rho b}\,; \end{cases}$$

the nonlinear error terms corresponding to the convection have the following decomposition:

(4.37e)
$$\begin{aligned} \mathcal{E}NLU&=\mathcal{N}_h(\boldsymbol{U},U)-\mathcal{N}_h(\boldsymbol{u},u)=\mathcal{N}_h(\tilde{\boldsymbol{u}},U)+\mathcal{N}_h(\boldsymbol{u},\tilde{u}), \\ \mathcal{E}NLV&=\mathcal{N}_h(\boldsymbol{U},V)-\mathcal{N}_h(\boldsymbol{u},v)=\mathcal{N}_h(\tilde{\boldsymbol{u}},V)+\mathcal{N}_h(\boldsymbol{u},\tilde{v}), \\ \mathcal{E}NLR&=\mathcal{N}_h(\boldsymbol{U},\Theta)-\mathcal{N}_h(\boldsymbol{u},\rho)=\mathcal{N}_h(\tilde{\boldsymbol{u}},\Theta)+\mathcal{N}_h(\boldsymbol{u},\tilde{\rho}). \end{aligned}$$

4.5.1. Preliminary results. The following preliminary results will be needed in the energy estimate of the system (4.37). The proofs are straightforward so that we omit the detail.

LEMMA 4.5. *We have the following:*

(i) *Inverse inequality in* 3*-D:*

(4.38a)
$$\|f\|_{L^\infty}\le\frac{C}{h^{\frac{3}{2}}}\|f\|_{L^2}.$$

(ii) *Suppose* $w_{i+1/2,j+1/2,0}=w_{i+1/2,j+1/2,N}$*; then*

(4.38b)
$$\|\overline{\overline{u}}\|_2\le\|u\|_1, \quad \|\overline{\overline{v}}\|_1\le\|v\|_2, \quad \|\overline{\overline{w}}\|_1\le\|w\|_3, \quad \|\overline{\overline{w}}\|_2\le\|w\|_3.$$

(iii) *For* $\tilde{w}$ *determined by* (4.37c)*, we have*

(4.38c)
$$\|\tilde{w}\|_3\le\|D_x^+\tilde{u}\|_1+\|D_y^+\tilde{v}\|_2.$$

(iv) *Suppose* $\tilde{\boldsymbol{v}}=(\tilde{u},\tilde{v})$ *and* $\tilde{\rho}$ *satisfy the boundary condition in* (4.37)*; then*

(4.38d)
$$\begin{aligned} &\|\tilde{D}_x\tilde{u}\|_1\le\|D_x^+\tilde{u}\|_1, \quad \|\tilde{D}_y\tilde{u}\|_1\le\|D_y^+\tilde{u}\|_1, \quad \|\tilde{D}_z\tilde{u}\|_1\le\|D_z^+\tilde{u}\|_1+h^4, \\ &\|\tilde{D}_y\tilde{v}\|_2\le\|D_y^+\tilde{v}\|_2, \quad \|\tilde{D}_x\tilde{v}\|_2\le\|D_x^+\tilde{v}\|_2, \quad \|\tilde{D}_z\tilde{v}\|_2\le\|D_z^+\tilde{v}\|+h^4, \\ &\|\tilde{D}_x\tilde{\rho}\|_3\le\|D_x^+\tilde{\rho}\|_3, \quad \|\tilde{D}_z\tilde{\rho}\|_3\le\|D_z^+\tilde{\rho}\|_3, \quad \|\tilde{D}_y\tilde{\rho}\|_3\le\|D_y^+\tilde{\rho}\|+h^4. \end{aligned}$$

(v) *Suppose* $w_{i+1/2,j+1/2,0} = w_{i+1/2,j+1/2,N} = 0$; *then*

$$\langle u, \tilde{D}_x p\rangle_1 + \langle v, \tilde{D}_y p\rangle_2 + \langle w, \tilde{D}_z p\rangle_3 = -\langle (\nabla_h \cdot \boldsymbol{v} + \tilde{D}_z w), p\rangle_4. \tag{4.38e}$$

4.5.2. Energy estimate for the error functions. Assume a priori that

$$\|\tilde{\boldsymbol{v}}\|_{L^\infty} + \|\tilde{w}\|_{L^\infty} \le \frac{1}{2}. \tag{4.39}$$

Such a priori assumption will be verified later using the inverse inequality (4.38a).

Taking the inner product of the first momentum error equation in (4.37a) with $\tilde{u}^{n+1}$ at the mesh point $(i, j+1/2, k+1/2)$, the second momentum error equation with $\tilde{v}^{n+1}$ at the mesh point $(i+1/2, j, k+1/2)$, the equation in (4.37b) with $\frac{\tilde{w}^{n+1}}{Ro}$ at the mesh point $(i+1/2, j+1/2, k)$, and summing up gives

(4.40)

$$\begin{aligned}
&\frac{1}{2}\cdot\frac{1}{\triangle t}\Big(\|\tilde{u}^{n+1}\|_1^2 - \|\tilde{u}^n\|_1^2 + \|\tilde{u}^{n+1}-\tilde{u}^n\|_1^2 + \|\tilde{v}^{n+1}\|_2^2 - \|\tilde{v}^n\|_2^2 + \|\tilde{v}^{n+1}-\tilde{v}^n\|_2^2\Big)\\
&+ \left\langle \tilde{u}^{n+1}, \mathcal{E}NLU^n \right\rangle_1 + \left\langle \tilde{v}^{n+1}, \mathcal{E}NLV^n \right\rangle_2 + \frac{1}{Ro}\Big(\langle \tilde{u}^{n+1}, -f\bar{\bar{\tilde{v}}}^n\rangle_1 + \langle \tilde{v}^{n+1}, f\bar{\bar{\tilde{u}}}^n\rangle_2\Big)\\
&+ \frac{1}{Ro}\Big(\langle \tilde{u}^{n+1}, D_x\tilde{p}^n\rangle_1 + \langle \tilde{v}^{n+1}, D_y\tilde{p}^n\rangle_2 + \langle \tilde{w}^{n+1}, D_z\tilde{p}^n\rangle_3\Big)\\
&- \left\langle \tilde{u}^{n+1}, (\nu_1\triangle_h + \nu_2 D_z^2)\tilde{u}^{n+1}\right\rangle_1 - \left\langle \tilde{v}^{n+1}, (\nu_1\triangle_h + \nu_2 D_z^2)\tilde{v}^{n+1}\right\rangle_2\\
&= \frac{1}{2}\cdot\frac{1}{\triangle t}\Big(\|\tilde{u}^{n+1}\|_1^2 - \|\tilde{u}^n\|_1^2 + \|\tilde{u}^{n+1}-\tilde{u}^n\|_1^2 + \|\tilde{v}^{n+1}\|_2^2 - \|\tilde{v}^n\|_2^2\\
&\qquad + \|\tilde{v}^{n+1}-\tilde{v}^n\|_2^2\Big) + I_{cu}^n + I_{cv}^n + \frac{1}{Ro}I_{cg}^n + \frac{1}{Ro}I_p^n + I_{du}^{n+1} + I_{dv}^{n+1}\\
&= \langle \tilde{u}^{n+1}, (\triangle t^3 + h^4)E^{u,n}\rangle_1 + \langle \tilde{v}^{n+1}, (\triangle t^3 + h^4)E^{v,n}\rangle_2\\
&\quad - \frac{1}{Ro}\langle \tilde{w}^{n+1}, \tilde{\rho}^n\rangle_3 + \frac{h^4}{Ro}\langle \tilde{w}^{n+1}, E^{p,n}\rangle_3.
\end{aligned}$$

A direct application of part (v) in Lemma 4.5 gives that I_p^n appearing in (4.40) vanishes indeed:

$$\begin{aligned}
I_p^n &= \langle \tilde{u}^{n+1}, D_x\tilde{p}^n\rangle_1 + \langle \tilde{v}^{n+1}, D_y\tilde{p}^n\rangle_2 + \langle \tilde{w}^{n+1}, D_z\tilde{p}^n\rangle_3\\
&= -\langle (\nabla_h\cdot\tilde{\boldsymbol{v}}^{n+1} + D_z\tilde{w}^{n+1}), \tilde{p}^n\rangle_4 = 0,
\end{aligned} \tag{4.41}$$

due to the fact that $\tilde{\boldsymbol{u}} = (\tilde{u}, \tilde{v}, \tilde{w})$ is identically divergence-free at the discrete level and the vertical velocity vanishes on the top and bottom boundaries. The identity (4.41) is analogous to (4.8), which shows that the 3-D velocity field is orthogonal to the pressure gradient in the staggered L^2 space. This represents the main advantage of the MAC grid.

The term I_{cg}^n, which corresponds to the Coriolis force, can be controlled directly by the Cauchy inequality and the application of part (ii) in Lemma 4.5:

(4.42)

$$|I_{cg}^n| = \left|\langle \tilde{u}^{n+1}, -f\bar{\bar{\tilde{v}}}^n\rangle_1 + \langle \tilde{v}^{n+1}, f\bar{\bar{\tilde{u}}}^n\rangle_2\right| \le \frac{f_0+\beta}{2}\Big(\|\tilde{u}^{n+1}\|_1^2 + \|\tilde{u}^n\|_1^2 + \|\tilde{v}^{n+1}\|_2^2 + \|\tilde{v}^n\|_2^2\Big).$$

Next we consider the terms I_{du}^{n+1}, I_{dv}^{n+1} corresponding to the diffusion of $\tilde{u}$ and $\tilde{v}$. A direct calculation shows that

$$-\langle \tilde{u}^{n+1}, D_x^2 \tilde{u}^{n+1}\rangle_1 = \|D_x^+ \tilde{u}^{n+1}\|_1^2, \quad -\langle \tilde{u}^{n+1}, D_y^2 \tilde{u}^{n+1}\rangle_1 = \|D_y^+ \tilde{u}^{n+1}\|_1^2, \tag{4.43a}$$

$$\begin{aligned} &-\langle \tilde{u}^{n+1}, D_z^2 \tilde{u}^{n+1}\rangle_1 = \|D_z \tilde{u}^{n+1}\|_1^2 + \mathcal{B}_{uz}^{n+1}, \\ &\mathcal{B}_{uz}^{n+1} = h^3 \sum_{j=0}^{N-1}\sum_{i=1}^{N-1}\Big(h^3 \tilde{u}_{i,j+1/2,1/2}^{n+1} \boldsymbol{e}_{ub} + h^3 \tilde{u}_{i,j+1/2,N-1/2}^{n+1} \boldsymbol{e}_{ut}\Big), \end{aligned} \tag{4.43b}$$

by utilizing the boundary condition for $\tilde{u}^{n+1}$ given in (4.37a). The boundary error term $\mathcal{B}_{uz}^{n+1}$ can be bounded from below as follows:

$$\begin{aligned} \mathcal{B}_{uz}^{n+1} &\geq h^3 \sum_{j=0}^{N-1}\sum_{i=1}^{N-1}\Big(-\frac{1}{2}(\tilde{u}_{i,j+1/2,1/2}^{n+1})^2 - \frac{1}{2}h^6 \boldsymbol{e}_{ub}^2 - \frac{1}{2}(\tilde{u}_{i,j+1/2,N-1/2}^{n+1})^2 - \frac{1}{2}h^6 \boldsymbol{e}_{ut}^2\Big) \\ &\geq -\frac{1}{2}\|\tilde{u}^{n+1}\|_1^2 - \frac{1}{2}h^9 \sum_{j=0}^{N-1}\sum_{i=1}^{N-1}(\boldsymbol{e}_{ub}^2 + \boldsymbol{e}_{ut}^2) \geq -\frac{1}{2}\|\tilde{u}^{n+1}\|_1^2 - \frac{1}{2}h^6\,; \end{aligned} \tag{4.44}$$

in the second step we absorbed the terms $\tilde{u}_{i,j+1/2,1/2}^2$ and $\tilde{u}_{i,j+1/2,N-1/2}^2$ into $\|\tilde{u}\|_1^2$ by its definition. Then we obtain

$$I_{du}^{n+1} \geq \nu_0(\|D_x^+ \tilde{u}^{n+1}\|_1^2 + \|D_y^+ \tilde{u}^{n+1}\|_1^2 + \|D_z^+ \tilde{u}^{n+1}\|_1^2) - \frac{1}{2}\nu_2 \|\tilde{u}^{n+1}\|_1^2 - \frac{1}{2}\nu_2 h^6, \tag{4.45}$$

in which $\nu_0 = \min(\nu_1, \nu_2, \kappa_1, \kappa_2)$. Similar estimates can be obtained for I_{dv}^{n+1}:

$$I_{dv}^{n+1} \geq \nu_0(\|D_x^+ \tilde{v}^{n+1}\|_2^2 + \|D_y^+ \tilde{v}^{n+1}\|_2^2 + \|D_z^+ \tilde{v}^{n+1}\|_2^2) - \frac{1}{2}\nu_2 \|\tilde{v}^{n+1}\|_2^2 - \frac{1}{2}\nu_2 h^6. \tag{4.46}$$

It remains to estimate I_{cu}^n and I_{cv}^n corresponding to the nonlinear convection terms. Using the decomposition for $\mathcal{E}NLU$ as shown in (4.37e) yields

$$I_{cu}^n = \Big\langle \tilde{u}^{n+1}, \mathcal{E}NLU^n \Big\rangle_1 = \Big\langle \tilde{u}^{n+1}, \mathcal{N}_h(\tilde{\boldsymbol{u}}^n, U^n) \Big\rangle_1 + \Big\langle \tilde{u}^{n+1}, \mathcal{N}_h(\boldsymbol{u}^n, \tilde{u}^n) \Big\rangle_1. \tag{4.47}$$

The application of the Cauchy inequality to the first integral appearing on the right-hand side of (4.47) indicates

$$-\Big\langle \tilde{u}^{n+1}, \mathcal{N}_h(\tilde{\boldsymbol{u}}^n, U^n) \Big\rangle_1 \leq \tilde{C}_1\Big(\|\tilde{u}^{n+1}\|_1^2 + \|\tilde{u}^n\|_1^2 + \|\overline{\tilde{v}}^n\|_1^2\Big) + \frac{2\tilde{C}_1^2}{\nu_0}\|\tilde{u}^{n+1}\|_1^2 + \frac{1}{8}\nu_0 \|\overline{\tilde{w}}^n\|_1^2, \tag{4.48}$$

where $\tilde{C}_1 = \|U\|_{W^{1,\infty}}$. The consistency analysis (4.35) shows that $\tilde{C}_1 \leq \|\boldsymbol{v}_e\|_{C^1} + 1$. Meanwhile, the combination of parts (ii) and (iii) in Lemma 4.5 gives

$$\|\overline{\tilde{w}}^n\|_1^2 \leq \|\tilde{w}^n\|_3^2 \leq 2(\|D_x^+ \tilde{u}^n\|^2 + \|D_y^+ \tilde{v}^n\|^2), \quad \|\overline{\tilde{v}}^n\|_1^2 \leq \|\tilde{v}^n\|_2^2, \tag{4.49}$$

whose insertion into (4.48) leads to

$$
\begin{aligned}
-\Big\langle \tilde{u}^{n+1}, \mathcal{N}_h(\tilde{\boldsymbol{u}}^n, U^n) \Big\rangle_1 &\le \frac{3\tilde{C}_1^2}{\nu_0}\|\tilde{u}^{n+1}\|_1^2 + \tilde{C}_1(\|\tilde{u}^n\|_1^2 + \|\tilde{v}^n\|_2^2) \\
&\quad + \frac{1}{4}\nu_0(\|D_x^+\tilde{u}^n\|_1^2 + \|D_y^+\tilde{v}^n\|_2^2).
\end{aligned} \tag{4.50}
$$

The second inner product appearing on the right-hand side of (4.47) can be controlled in a similar way:

$$
-\Big\langle \tilde{u}^{n+1}, \mathcal{N}_h(\boldsymbol{u}^n, \tilde{u}^n) \Big\rangle_1 \le 2\cdot\frac{\tilde{C}_2^2}{\nu_0}\|\tilde{u}^{n+1}\|_1^2 + \frac{1}{4}\nu_0\Big(\|D_x^+\tilde{u}^n\|_1^2 + \|D_y^+\tilde{u}^n\|_1^2 + \|D_z^+\tilde{u}^n\|_1^2\Big), \tag{4.51}
$$

where $\tilde{C}_2 = \|\boldsymbol{u}\|_{L^\infty}$. The a priori assumption (4.39) and the consistency analysis (4.35) assures that

$$
\tilde{C}_2 \le \|\boldsymbol{V}\|_{L^\infty} + \|\boldsymbol{W}\|_{L^\infty} + \frac{1}{2} \le \|\boldsymbol{u}_e\|_{C^0} + C(\triangle t + h^2) + \frac{1}{2} \le \|\boldsymbol{u}_e\|_{C^0} + 1, \tag{4.52}
$$

provided that $\triangle t$ and h are small enough. Applying part (iv) of Lemma 4.5 into (4.52) results in

$$
\begin{aligned}
&-\Big\langle \tilde{u}^{n+1}, \mathcal{N}_h(\boldsymbol{u}^n, \tilde{u}^n) \Big\rangle_1 \\
&\quad\le \frac{2\tilde{C}_2^2}{\nu_0}\|\tilde{u}^{n+1}\|_1^2 + \frac{1}{4}\nu_0\Big(\|D_x^+\tilde{u}^n\|_1^2 + \|D_y^+\tilde{u}^n\|^2 + \|D_z^+\tilde{u}^n\|_1^2 + 2h^6\Big).
\end{aligned} \tag{4.53}
$$

Thus the combination of (4.51) and (4.53) gives

$$
\begin{aligned}
I_{cu}^n &\ge -\Big(\frac{3\tilde{C}_1^2}{\nu_0} + \frac{2\tilde{C}_2^2}{\nu_0}\Big)\|\tilde{u}^{n+1}\|_1^2 - \tilde{C}_1(\|\tilde{u}^n\|_1^2 + \|\tilde{v}^n\|_2^2) \\
&\quad - \frac{1}{2}\nu_0\Big(\|D_x^+\tilde{u}^n\|_1^2 + \|D_y^+\tilde{u}^n\|_1^2 + \|D_z^+\tilde{u}^n\|_1^2\Big) - h^6,
\end{aligned} \tag{4.54}
$$

where $\tilde{C}_1 \le \|\boldsymbol{v}_e\|_{C^1}+1$, $\tilde{C}_2 \le \|\boldsymbol{u}_e\|_{C^0}+1$. The bound for I_{cv}^n can be similarly obtained:

$$
\begin{aligned}
I_{cv}^n &\ge -\Big(\frac{3\tilde{C}_1^2}{\nu_0} + \frac{2\tilde{C}_2^2}{\nu_0}\Big)\|\tilde{v}^{n+1}\|_2^2 - \tilde{C}_1(\|\tilde{u}^n\|_1^2 + \|\tilde{v}^n\|_2^2) \\
&\quad - \frac{1}{2}\nu_0\Big(\|D_x^+\tilde{v}^n\|_2^2 + \|D_y^+\tilde{v}^n\|_2^2 + \|D_z^+\tilde{v}^n\|_2^2\Big) - h^6.
\end{aligned} \tag{4.55}
$$

The four terms appearing on the right-hand side of (4.40) can be controlled by the Cauchy inequality, together with the application of part (iii) of Lemma 4.5:

$$
\begin{aligned}
&\langle \tilde{u}^{n+1}, (\triangle t^3 + h^4)E^{u,n}\rangle_1 \le \frac{1}{2}\|\tilde{u}^{n+1}\|_1^2 + (\triangle t^6 + h^8)\|E^{u,n}\|_1^2, \\
&\langle \tilde{v}^{n+1}, (\triangle t^3 + h^4)E^{v,n}\rangle_2 \le \frac{1}{2}\|\tilde{v}^{n+1}\|_2^2 + (\triangle t^6 + h^8)\|E^{v,n}\|_2^2, \\
&-\frac{1}{Ro}\langle \tilde{w}^{n+1}, \tilde{\rho}^n\rangle_3 \le \frac{1}{8}\nu_0(\|D_x^+\tilde{u}^{n+1}\|^2 + \|D_y^+\tilde{v}^{n+1}\|^2) + \frac{C}{\nu_0}\|\tilde{\rho}^n\|_3^2, \\
&\frac{h^4}{Ro}\langle \tilde{w}^{n+1}, E^{p,n}\rangle_3 \le \frac{1}{8}\nu_0(\|D_x^+\tilde{u}^{n+1}\|_1^2 + \|D_y^+\tilde{v}^{n+1}\|_2^2) + \frac{C}{\nu_0}h^8\,\|E^{p,n}\|_3^2.
\end{aligned} \tag{4.56}
$$

Substituting (4.56), (4.55), (4.54), (4.46), (4.45), (4.42), and (4.41) into (4.40), and denoting

$$\begin{aligned}\mathcal{I}EV &= \|D_x^+\tilde{u}\|_1^2 + \|D_y^+\tilde{u}\|_1^2 + \|D_z^+\tilde{u}\|_1^2 + \|D_x^+\tilde{v}\|_2^2 + \|D_y^+\tilde{v}\|_2^2 + \|D_z^+\tilde{v}\|_2^2,\\ \mathcal{I}ER &= \|D_x^+\tilde{\rho}\|_3^2 + \|D_y^+\tilde{\rho}\|_3^2 + \|D_z^+\tilde{\rho}\|_3^2,\end{aligned} \tag{4.57}$$

we have the energy estimate for $\tilde{\boldsymbol{v}}$

$$\begin{aligned}&\frac{1}{2}\cdot\frac{1}{\triangle t}\Big(\|\tilde{u}^{n+1}\|_1^2 - \|\tilde{u}^n\|_1^2 + \|\tilde{v}^{n+1}\|_2^2 - \|\tilde{v}^n\|_2^2\Big) + \frac{3}{4}\nu_0\mathcal{I}EV^{n+1}\\ &\le \Big(\frac{4\tilde{C}_1^2}{\nu_0} + \frac{4\tilde{C}_2^2}{\nu_0} + C\Big)\|\tilde{\boldsymbol{v}}\|^2 + \frac{C}{\nu_0}\|\tilde{\rho}\|_3^2 + \frac{1}{2}\nu_0\mathcal{I}EV^n + \tilde{E}_u^n,\end{aligned} \tag{4.58a}$$

in which $\tilde{C}_1 \le \|\boldsymbol{v}_e\|_{C^1} + 1$, $\tilde{C}_2 \le \|\boldsymbol{u}_e\|_{C^0} + 1$, and the error term satisfies

$$\tilde{E}_u^n \le \frac{1}{2}(\triangle t^6 + h^8)\Big(\|E^{u,n}\|_1^2 + \|E^{v,n}\|_2^2) + \frac{\|E^{p,n}\|_3^2}{\nu_0}\Big) + Ch^6. \tag{4.58b}$$

The energy estimate for the density error function can be carried out in a similar way (we omit the details):

$$\begin{aligned}\frac{1}{2}\cdot\frac{1}{\triangle t}\Big(\|\tilde{\rho}^{n+1}\|_3^2 - \|\tilde{\rho}^n\|_3^2\Big) + \frac{3}{4}\nu_0\mathcal{I}ER^{n+1} &\le \Big(\frac{\tilde{C}_3^2}{\nu_0} + \frac{4\tilde{C}_2^2}{\nu_0} + C\Big)\|\tilde{\rho}\|_3^2 + \frac{1}{2}\|\tilde{\boldsymbol{v}}\|^2\\ &+ \frac{1}{8}\nu_0(\|D_x^+\tilde{u}^n\|_1^2 + \|D_y^+\tilde{v}^n\|_2^2) + \frac{1}{2}\nu_0\mathcal{I}ER^n + C(\triangle t^6 + h^8)\,\|E^{\rho,n}\|_3^2,\end{aligned} \tag{4.59}$$

in which $\tilde{C}_3 = \|\Theta\|_{W^{1,\infty}} \le \|\rho_e\|_{C^1} + 1$. By setting $\|\tilde{\boldsymbol{v}}\|^2 = \|\tilde{u}\|_1^2 + \|\tilde{v}\|_2^2$, we arrive at

$$\begin{aligned}&\frac{1}{2}\cdot\frac{1}{\triangle t}\Big(\|\tilde{\boldsymbol{v}}^{n+1}\|^2 - \|\tilde{\boldsymbol{v}}^n\|^2 + \|\tilde{\rho}^{n+1}\|_3^2 - \|\tilde{\rho}^n\|_3^2\Big) + \frac{3}{4}\nu_0\,\mathcal{I}EV^{n+1} + \frac{3}{4}\nu_0\,\mathcal{I}ER^{n+1}\\ &\le \Big(\frac{4\tilde{C}_1^2}{\nu_0} + \frac{4\tilde{C}_2^2}{\nu_0} + \frac{\tilde{C}_3^2}{\nu_0} + C\Big)(\|\tilde{\boldsymbol{v}}\|^2 + \|\tilde{\rho}\|_3^2) + \frac{5}{8}\nu_0\,\mathcal{I}EV^n + \frac{1}{2}\nu_0\,\mathcal{I}ER^n + \tilde{E}^n, \text{ with}\\ &\tilde{E}^n \le C(\triangle t^6 + h^8)\Big(\|E^{u,n}\|_1^2 + \|E^{v,n}\|_2^2 + \|E^{\rho,n}\|_3^2) + \frac{\|E^{p,n}\|_3^2}{\nu_0}\Big) + Ch^6,\end{aligned} \tag{4.60}$$

since the term $(\|D_x^+\tilde{u}^n\|_1^2 + \|D_y^+\tilde{v}^n\|_2^2)$ appearing on the right-hand side of (4.59) can be absorbed into $\mathcal{I}EV^n$. Summing (4.60) in time and applying the Gronwall inequality yield

$$\|\tilde{\boldsymbol{v}}^n\|^2 + \|\tilde{\rho}^n\|_3^2 \le \quad C\cdot\exp\Big(\frac{Ct}{\nu_0}\Big)\Big(\triangle t^6 + h^8\Big)(\mathcal{C}^*)^2 + CTh^6, \tag{4.61}$$

where C was given in Theorem 4.1 and $\mathcal{C}^*$ depends only on the exact solution. In the derivation of (4.61), we drop the gradient terms since the coefficients of $\mathcal{I}EV$, $\mathcal{I}ER$ on the right-hand side of (4.60) are less than those on the left-hand side. The inequality (4.61) amounts to saying

$$\begin{aligned}&\|\boldsymbol{v}_{\triangle t,h} - \boldsymbol{V}\|_{L^\infty(0,T;\boldsymbol{L}_h^2)} + \|\rho_{\triangle t,h} - \Theta\|_{L^\infty(0,T;L_h^2)}\\ &\le C\mathcal{C}^*\Big(\exp\Big\{\frac{CT}{\nu_0}\Big\} + T\Big)\Big(\triangle t^3 + h^3\Big),\end{aligned} \tag{4.62}$$

whose combination with the estimate (4.35) gives the convergence result (4.3a). The inverse inequality in three dimensions as given in Lemma 4.5 shows that

$$\|\tilde{\boldsymbol{v}}\|_{L^\infty} \leq C\frac{\triangle t^3 + h^3}{h^{\frac{3}{2}}}, \tag{4.63}$$

and this is bounded by $Ch^{3/2}$, since we impose to $\triangle t$ a CFL-like condition $\triangle t \leq Ch$. Moreover, we have

$$\|\tilde{w}\|_{L^\infty} \leq \frac{C}{h}\|\tilde{\boldsymbol{v}}\|_{L^\infty} \leq Ch^{1/2}, \tag{4.64}$$

which comes from the determination identity for $\tilde{w}$ in (4.37). As a result, the a priori assumption (4.39) is satisfied if h is small enough. Thus Theorem 4.1 is proven.

Remark 4.6. The inverse inequality (4.38a) recovers the L^∞ a priori assumption (4.39) for the velocity field. This is the main advantage in the analysis of the fully discretized system. Since the vertical velocity is formulated as the integration of the divergence for the horizontal velocity, the $O(h^{\frac{5}{2}})$ estimate for the L^2 norm of $\tilde{\boldsymbol{v}}$ is required. This is the reason for the higher order consistency analysis in section 4.4.

Remark 4.7. The stability constraint in Theorem 4.1 is $\triangle t \leq Ch$. We infer from (4.62) that the backward Euler scheme is unconditionally stable for the $L^2(0,T;L^2)$ norm, as expected from a scheme with implicit treatment of the diffusion term. The stability constraint $\triangle t \leq Ch$ is introduced after (4.63), (4.64) to recover the $L^\infty([0,T]\times\mathcal{M})$ stability, and C is an arbitrary fixed constant; note that the usual CFL constraint has the same form with $C = |\boldsymbol{u}|_{L^\infty}^{-1}$, but in the present case C is arbitrary, since the CFL condition is needed only to ensure additional stability.

5. Numerical accuracy check. In this section we check the numerical accuracy of the computational scheme. The exact velocity and density are chosen to be

$$\begin{aligned} u_e(x,y,z,t) &= \frac{1}{\pi^2}\sin(\pi x)\sin(\pi y)\cos(\pi z)\cos t, \\ v_e(x,y,z,t) &= \frac{1}{\pi^2}\sin(\pi x)\sin(\pi y)\cos(\pi z)\cos t, \\ \rho_e(x,y,z,t) &= \frac{1}{\pi^2}\cos(\pi x)\cos(\pi y)\cos(\pi z)\cos t. \end{aligned} \tag{5.1}$$

The corresponding exact vertical velocity w_e and exact pressure variable p_e are determined by the incompressibility $\nabla\cdot\boldsymbol{v}_e + \partial_z w_e$ and hydrostatic balance $\frac{\partial p_e}{\partial z} = -\rho_e$, respectively:

$$\begin{aligned} w_e(x,y,z,t) &= -\frac{1}{\pi^2}\Big(\cos(\pi x)\sin(\pi y) + \sin(\pi x)\cos(\pi y)\Big)\sin(\pi z)\cos t, \\ p_e(x,y,z,t) &= \frac{1}{\pi^3}\cos(\pi x)\cos(\pi y)\Big(1 - \sin(\pi z)\Big)\cos t, \end{aligned} \tag{5.2}$$

in which we set the exact surface pressure as

$$p_{se}(x,y,t) = p_e(x,y,0,t) = \frac{1}{\pi^3}\cos(\pi x)\cos(\pi y)\cos t. \tag{5.3}$$

TABLE 5.1

Error and order of accuracy for velocity and density at $t = 1$ when the Crank–Nicolson *scheme using* MAC *spatial discretization is used. $\triangle t = \frac{1}{4}\triangle x$. The physical parameters: Rossby number $Ro = 0.5$, Coriolis force $f = 0.5 + y$.*

	N	L^1 error	L^1 order	L^2 error	L^2 order	L^∞ error	L^∞ order
u	16	6.67e-05		9.15e-05		3.50e-04	
	32	1.66e-05	2.00	2.29e-05	1.99	9.06e-05	1.95
	64	4.15e-06	2.00	5.71e-06	2.00	2.29e-05	1.98
	128	1.03e-07	2.01	1.43e-06	2.00	5.73e-06	2.00
v	16	2.56e-04		3.78e-04		1.28e-03	
	32	6.40e-05	2.00	9.46e-05	1.99	3.23e-04	1.99
	64	1.60e-06	2.00	2.37e-05	2.00	8.10e-05	2.00
	128	4.01e-06	2.00	5.93e-06	2.00	2.03e-05	2.00
ρ	16	4.78e-05		6.17e-05		2.01e-04	
	32	1.19e-05	2.00	1.54e-05	2.00	5.22e-05	1.95
	64	2.98e-06	2.00	3.68e-06	2.00	1.32e-05	1.98
	128	7.48e-07	1.99	9.68e-07	2.00	3.30e-06	2.00

Then we arrive at the following system of PEs with force terms $\boldsymbol{f}$, $\boldsymbol{g}$ in the momentum equation and the density equation

(5.4a)
$$\begin{cases} \partial_t \boldsymbol{v}_e + (\boldsymbol{v}_e \cdot \nabla)\boldsymbol{v}_e + w_e \dfrac{\partial \boldsymbol{v}_e}{\partial z} + \dfrac{1}{Ro}\Big(fk \times \boldsymbol{v}_e + \nabla p_e\Big) = \Big(\nu_1 \triangle + \nu_1 \partial_z^2\Big)\boldsymbol{v}_e + \boldsymbol{f}, \\ \dfrac{\partial p_e}{\partial z} = -\rho_e, \\ \nabla \cdot \boldsymbol{v}_e + \partial_z w_e = 0, \\ \partial_t \rho_e + (\boldsymbol{v}_e \cdot \nabla)\rho_e + w_e \dfrac{\partial \rho_e}{\partial z} = \Big(\kappa_1 \triangle + \kappa_2 \partial_z^2\Big)\rho_e + \boldsymbol{g}, \end{cases}$$

with the boundary condition

(5.4b)
$$\begin{aligned} &\frac{\partial \boldsymbol{v}_e}{\partial z} = 0, \quad w_e = 0, \quad \frac{\partial \rho_e}{\partial z} = 0 \quad \text{at } z = 0, -H_0, \\ &\boldsymbol{v}_e = 0, \quad \frac{\partial \rho_e}{\partial \boldsymbol{n}} = 0 \quad \text{on} \quad \partial\mathcal{M}_0 \times [-H_0, 0]. \end{aligned}$$

The computational domain is chosen as $\mathcal{M} = \mathcal{M}_0 \times [-H_0, 0]$, where $\mathcal{M}_0 = [0,1]^2$, $H_0 = 1$. The viscosity parameters are given by $\nu_1 = \nu_2 = 0.005$, $\kappa_1 = \kappa_2 = 0.005$. In a usual GFD model, the Rossby number ranges from $O(1)$ to $O(10^{-3})$. We choose $Ro = 0.5$ in the numerical experiment. The Coriolis force parameter is set to be $f_0 = 0.5$, $\beta = 1$.

The system (5.4) can be formulated in the same fashion as (1.13) such that the surface pressure Poisson equation replaces the nonlocal incompressibility constraint for the horizontal velocity. Note that a force term $\nabla \cdot \boldsymbol{f}$ appears in the Poisson equation. Based on such formulation, we apply the Crank–Nicolson method, a second order numerical scheme with implicit diffusion terms, using the MAC spatial grid, to solve the PEs (5.4). The force terms $\boldsymbol{f}$, $\boldsymbol{g}$ and $\nabla \cdot \boldsymbol{f}$ are added when we update the momentum equation and the density equation and solve the surface pressure Poisson equation. The final time is taken to be $t = 1.0$. Table 5.1 lists the absolute errors between the numerical and exact solutions for velocity and density. All the error functions are measured in L^1, L^2, and L^∞ norms in a discrete level similar to that

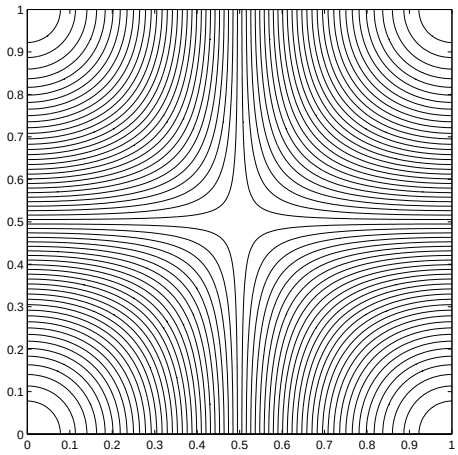

FIG. 5.1. *The contour plot of the surface pressure at* $t = 1$ *with* $N = 128$.

in the notation (4.2). As can be seen, exactly second order accuracy for the velocity field $\boldsymbol{v} = (u, v)$ and the density field ρ, in both L^1, L^2, and L^∞ norms, is obtained.

The contour plot of the surface pressure at the final time $t = 1.0$ (calculated by the resolution $N = 128$) is also presented in Figure 5.1, which shows a smooth numerical profile and verifies the robustness of the computational method. Such a plot gives an accurate approximation to the exact surface pressure given by (5.3).

Acknowledgment. The authors are grateful to the referees for their insightful comments.

REFERENCES

[1] A. S. ALMGREN, J. B. BELL, AND W. G. SZYMCZAK, *A numerical method for the incompressible Navier–Stokes equations based on an approximate projection*, SIAM J. Sci. Comput., 17 (1996), pp. 358–369.

[2] A. J. CHORIN, *Numerical solution of the Navier-Stokes equations*, Math. Comp., 22 (1968), pp. 745–762.

[3] J. K. DUKOWICZ AND R. D. SMITH, *A reformulation and implementation of Bryan-Cox-Semtner ocean model on the connection machine*, J. Atmos. Oceanic Tech., 10 (1993), pp. 195–208.

[4] W. E AND J.-G. LIU, *Projection method* I: *Convergence and numerical boundary layers*, SIAM J. Numer. Anal., 32 (1995), pp. 1017–1057.

[5] W. E AND J.-G. LIU, *Projection method* II: *Godunov–Ryabenski analysis*, SIAM J. Numer. Anal., 33 (1996), pp. 1597–1621.

[6] W. E AND J.-G. LIU, *Vorticity boundary condition and related issues for finite difference schemes*, J. Comput. Phys., 124 (1996), pp. 368–382.

[7] W. E AND J.-G. LIU, *Projection method* III: *Spatial discretization on the staggered grid*, Math. Comp., 71 (2002), pp. 27–47.

[8] P. GRESHO AND R. SANI, *On pressure boundary conditions for the incompressible Navier-Stokes equations*, Internat. J. Numer. Methods Fluids, 7 (1987), pp. 1111–1145.

[9] F. HARLOW AND J. WELCH, *Numerical calculation of time-dependent viscous incompressible flow of fluid with free surface*, Phys. Fluids, 8 (1965), pp. 2182–2189.

[10] T. Y. HOU AND B. T. R. WETTON, *Convergence of a finite difference scheme for the Navier–Stokes equations using vorticity boundary conditions*, SIAM J. Numer. Anal., 29 (1992), pp. 615–639.

[11] H. E. JOHNSTON AND J.-G. LIU, *Finite difference schemes for incompressible flow based on local pressure boundary conditions*, J. Comput. Phys., 180 (2002), pp. 120–154.

[12] J. L. LIONS, R. TEMAM, AND S. WANG, *New formulations of the primitive equations of the atmosphere and applications*, Nonlinearity, 5 (1992), pp. 237–288.

[13] J. L. Lions, R. Temam, and S. Wang, *On the equations of large-scale ocean*, Nonlinearity, 5 (1992), pp. 1007–1053.
[14] J. L. Lions, R. Temam, and S. Wang, *Models for the coupled atmosphere and ocean (CAO* I*)*, Comput. Mech. Adv., 1 (1993), pp. 3–54.
[15] J. L. Lions, R. Temam, and S. Wang, *Numerical analysis of the coupled atmosphere and ocean models (CAO*II*)*, Comput. Mech. Adv., 1 (1993), pp. 55–120.
[16] J. L. Lions, R. Temam, and S. Wang, *Mathematical problems of the coupled models of atmosphere and ocean (CAO*III*)*, J. Math. Pures Appl. (9), 74 (1995), pp. 105–163.
[17] S. Orszag and M. Israeli, *Numerical simulation of viscous incompressible flow*, Annu. Rev. Fluid Mech., 6 (1974), pp. 281–318.
[18] S. Orszag and M. Israeli, *Boundary conditions for incompressible flows*, J. Sci. Comput., 1 (1986), pp. 75–111.
[19] J. Pedlosky, *Geophysical Fluid Dynamics*, 2nd ed., Springer-Verlag, New York, 1987.
[20] N. Pinardi, A. Rosati, and R. C. Pacanowski, *The sea surface pressure formulation of frigid lid models. Implications for altimetric data assimilation studies*, J. Marine Systems, 6 (1995), pp. 109–119.
[21] J. Shen, *On error estimates of projection methods for Navier–Stokes equations: First-order schemes*, SIAM J. Numer. Anal., 29 (1992), pp. 57–77.
[22] J. Shen, *On error estimates of some higher order projection and penalty-projection methods for Navier-Stokes equations*, Numer. Math., 62 (1992), pp. 49–73.
[23] J. Shen and S. Wang, *A fast and accurate numerical scheme for the primitive equations of the atmosphere*, SIAM J. Numer. Anal., 36 (1999), pp. 719–737.
[24] R. D. Smith, J. K. Dukowicz, and R. C. Malone, *Parallel ocean general circulation modeling*, Phys. D, 60 (1992), pp. 38–61.
[25] R. Temam, *Sur l'approximation de la solution des equations Navier-Stokes par la méthode des fractionnarires ii*, Arch. Rational Mech. Anal., 33 (1969), pp. 377–385.
[26] R. Temam, *Navier Stokes Equations: Theory and Numerical Analysis*, North-Holland, Amsterdam, 1984.
[27] A. Thom, *The flow past circular cylinders at low speeds*, Proc. Roy. Soc. London Ser. A, 141 (1933), pp. 651–669.
[28] C. Wang and J.-G. Liu, *Analysis of finite difference schemes for unsteady Navier-Stokes equations in vorticity formulation*, Numer. Math., 91 (2002), pp. 543–576.